UNIVERSITY OF TURKU

Chick Chorioallantoic Membrane as a Model for Glioblastoma Growth, Invasion and Treatment

Institute of Biomedicine
MDP in Biomedical Sciences
Drug Discovery and Development
Master's thesis

Author:
Aleksi Hakkarainen

Supervisors:
Milena Doroszko, PhD, Uppsala University
Adjunct Professor Petra Sipilä, PhD, University of Turku

24.11.2025
Uppsala & Turku

Master's thesis

Subject: Drug Discovery and Development
Author: Aleksi Hakkarainen
Title: Chick Chorioallantoic Membrane as a Model for Glioblastoma Growth, Invasion and Treatment
Supervisor(s): Milena Doroszko, PhD, Uppsala University; Adjunct Professor Petra Sipilä, PhD, University of Turku
Number of pages: 62 pages, 3 Appendices
Date: 24.11.2025

Glioblastoma is the most aggressive primary brain tumour, with a median patient survival of only 15 months. Its rapid proliferation, high invasion, poor therapeutic response, and recurrence, combined with substantial inter- and intra-tumoural heterogeneity, complicate the development of efficient therapies and highlight the need for personalised treatment strategies. Personalised treatment strategies require rapid and efficient experimental models capable of capturing diverse tumour behaviours. The chick chorioallantoic membrane (CAM) model represents a promising intermediate platform between *in vitro* assays and rodent xenografts. This thesis evaluated the suitability of the CAM model for studying glioblastoma tumour growth, invasion, and treatment response using 17 patient-derived Human Glioblastoma Cell Culture (HGCC) cell lines.

All 17 cell lines formed tumours with high xenografting efficiency (> 90%), demonstrating that the CAM environment efficiently supports tumour development. Histological analyses revealed morphological heterogeneity and variation in invasion levels, reflecting the heterogeneity of glioblastoma phenotypes. The CAM vasculature consistently formed around the tumours, further supporting glioblastoma growth. Ki67 immunostaining confirmed active proliferation across all xenografts, with proliferation rates varying between cell lines. High Nestin expression demonstrated preservation of glioblastoma stem/progenitor like characteristics in the CAM model. Tumour weight analysis revealed variable tumour growth progression, underlining limitations of weight-based growth assessment.

To evaluate the CAM model's suitability for drug screening, nine GFP-Luc labelled HGCC cell lines were treated with the proteasome inhibitor bortezomib, previously identified as a potent agent against glioblastoma in large-scale drug screening. Due to the limitations in weight-based growth assessment, bioluminescence imaging (BLI) was used before and after the treatment to accurately monitor treatment responses. The change in cellular viability in response to bortezomib treatment was analysed by calculating relative change in BLI signal intensity for each group. Five cell lines exhibited significant decrease in cellular viability, whereas four cell lines showed resistance against the treatment. These sensitivity patterns aligned with *in vitro* and mouse xenograft results, supporting the translational relevance of CAM based drug testing.

Overall, this study demonstrates that the CAM model enables efficient glioblastoma tumour formation and analysis of tumour growth and invasion. The CAM model holds promise as an effective model for glioblastoma treatment screening and has potential as a bridge between large-scale *in vitro* drug screening and mammalian *in vivo* studies. The short experimental timeline of the CAM model is both an advantage and a limitation. It enables rapid results, which is an important characteristic of a model for patient-specific treatment testing, but the short duration does not enable long-term studies of tumour progression and treatment effects. Additional research is needed to further optimise the CAM model for glioblastoma studies and drug screening.

Key words: glioblastoma, CAM model, xenograft, HGCC cell line, proteasome inhibition, bortezomib.

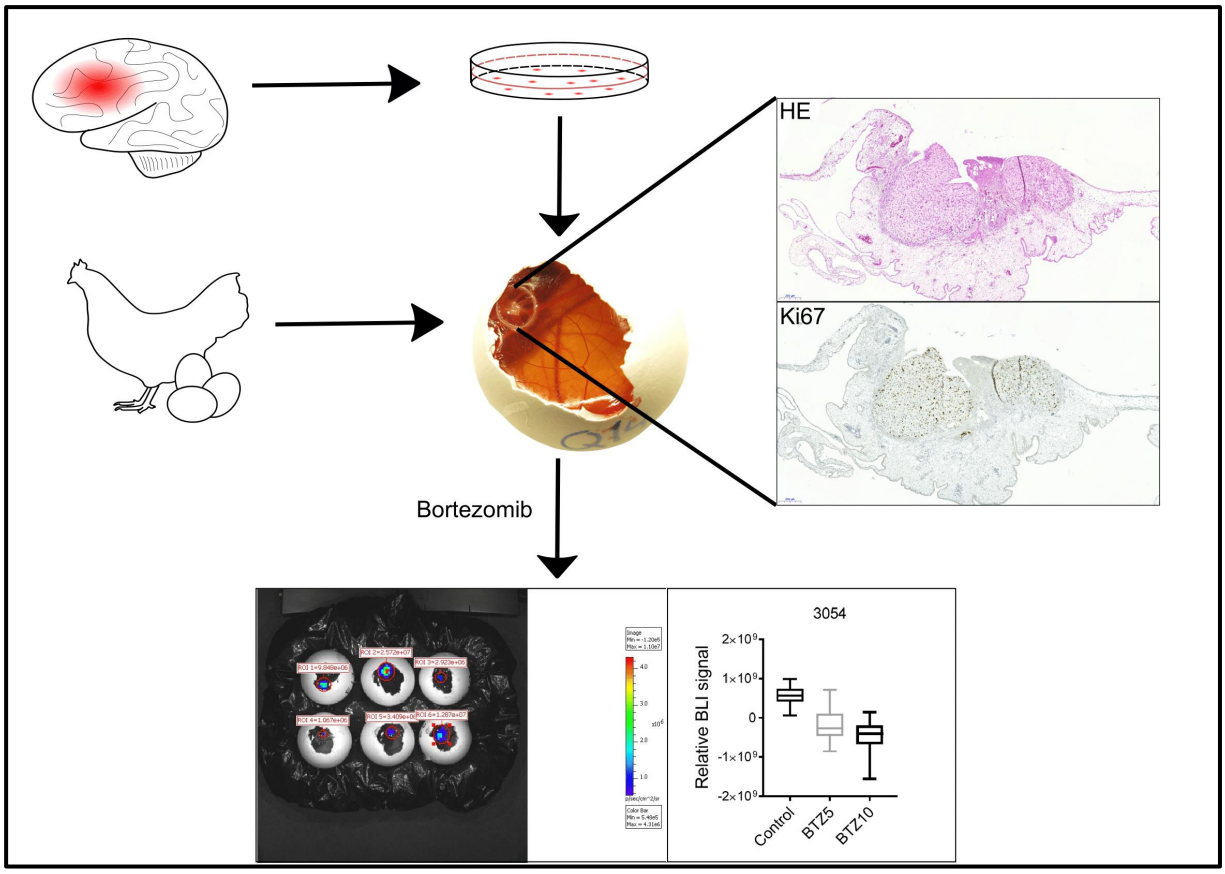
HE
Ki67
Bortezomib
3054
Relative BLI signal
2×10⁹
1×10⁹
0
-1×10⁹
-2×10⁹
Control
BTZ5
BTZ10

Table of contents

1 INTRODUCTION

1.1 Glia cells

Glial cells are non-neuronal cells in the central nervous system (CNS), and they have supportive and protective roles in neuron function and are crucial for normal neurotransmission in CNS. There are three main types of glial cells in CNS: astrocytes, oligodendrocytes, and microglia. Astrocytes, the most abundant glial cell type, support neuronal function by maintaining homeostasis, regulating synaptic transmission, and modulating blood flow (Liu et al., 2021). Oligodendrocytes are responsible for forming and maintaining myelin sheath around neural axons, which potentiates signal transmission between neurons (Zhang et al., 2025). Microglia function as the first line immune defence in the CNS and have structural and functional similarities with macrophages (Colonna & Butovsky, 2017). They monitor the brain environment, remove cellular debris, and respond to injury or infection by releasing inflammatory signals. Additionally, they help regulate synaptic connections and contribute to brain development and repair (Cornell et al., 2021). Uncontrollable growth of glial cells forms gliomas, which vary in aggressiveness and prognosis.

1.2 Glioblastoma

Gliomas are the most common primary brain tumours that originate from the glial cells of the brain or spinal cord. It's a broad category of tumours that cover 28% of all brain tumours and 80% of malignant ones. Glioblastoma, the most aggressive type of gliomas, accounts for over 50% of all malignant brain tumours and 16% of all primary brain tumours (Ostrom et al., 2013). Glioblastoma is characterised by rapid proliferation, extensive infiltration, and resistance to therapy. Despite advancements in surgery, radiotherapy, and chemotherapy, patient prognosis remains poor. The highly heterogeneous nature of glioblastoma, coupled with its complex genetic and molecular landscape, presents significant challenges in treatment development.

Glioblastoma is most often located in the supratentorial region (*i.e.* frontal, temporal parietal, and occipital lobes) (Chakrabarti et al., 2005), while tumours in cerebellum or spinal cord are rare (Adams et al., 2013; Engelhard et al., 2010). Due to the strong invasive nature of glioblastoma, it is not always restricted to one area of the brain.

1.2.1 Incidence rate of glioblastoma

The incidence rate (IR) of glioblastoma has a great variation between countries. The international age-adjusted IR is approximately between 0.77 and 4.8 per 100 000 persons (Grochans et al., 2022). Glioblastoma IRs in Finland and the United States are 2.9 – 3.5 per 100 000 (Korja et al., 2018; Natukka et al., 2019) persons and 3.27 per 100 000 persons (Ostrom et al., 2023), respectively. Like in other types of cancer, an increase in global incidence of brain and CNS tumours, including glioblastoma, has been reported (Miranda-Filho et al., 2016).

Like mentioned above, global variation in glioblastoma incidence rate between countries is significant, even though it needs to be noted that numerical incidence rates are not fully comparable due to the different methodologies used in calculating the data. European and North-American countries show in general higher glioblastoma IR than Asian countries (Table 1). The glioblastoma incidence data from Africa and South America is less comprehensive, but some studies indicate the IR to be lower than in Europe and North America (Ballard et al., 2024). In the United States the IR of glioblastoma is two-fold in the European-American population compared to African-American population (3.45 versus 1.67 per 100 000) (Ostrom et al., 2013). The IR in Non-Hispanic population is higher (3.26 per 100 000) than in Hispanic population (2.45 per 100 000). The IR variation based on region and ethnicity highlight the effect of environmental and genetic factors behind glioblastoma.

Globally, glioblastoma IR is 1.6 times higher in male population compared to the female population (Carrano et al., 2021). In the United States glioblastoma has an IR of 4.09 per 100 000 in males versus 2.55 per 100 000 in females (Ostrom et al., 2023). In Finland, 42% of glioblastoma cases were in the female population between 2000 and 2013 (Korja et al., 2018).

Table 1. Reported glioblastoma incidence rates in countries with accessible epidemiological data.

Country	Reference	Years	Incidence rate (per 100 000)
Croatia	(Dobec-Meić et al., 2006)	1996 – 2004	4.8
England	(Brodbelt et al., 2015)	2007 – 2011	4.64
Canada	(Walker et al., 2019)	2009 – 2013	4.06
Australia	(Dobes et al., 2011)	2000 – 2008	3.96
The United States	(Ostrom et al., 2023)	2016 – 2020	3.27
Finland	(Natukka et al., 2019) (Korja et al., 2018)	2007 – 2016 2000 – 2013	3.5 2.9
Japan	(Miyakoshi et al., 2024)	2012 – 2021	2.1
Republic of Korea	(Jung et al., 2013) (Dho et al., 2017)	2010 2013	0.77 0.87

1.2.2 Current treatment of glioblastoma

Surgery is the primary therapeutic approach for glioblastoma. The goal of the surgery is to perform maximal safe resection. Due to the invasive nature of glioblastoma, all the tumour cells cannot be removed with surgery. Thus, the surgery in glioblastoma patients is always balancing between maximal removal of tumour and the preservation of normal brain function. It is shown that remaining tumour cells post-surgery leads to later disease progression and recurrence (Wilson et al., 2014). For glioblastoma the most important treatment-related survival predictor is extent of resection (EOR) (Wolbers, 2014). High EOR is associated with better life expectancy and longest survival is seen in patients with gross total resection surgery and following radiotherapy and chemotherapy with temozolomide (Wilson et al., 2014).

Chemotherapies are most often ineffective against glioblastoma cells due to extraordinary capability to evade apoptosis (Singh et al., 2025). Temozolomide (TMZ) is the only chemotherapy that has shown limited potential against glioblastoma, but only in a specific group of patients (Wick et al., 2012). TMZ is an oral alkylating agent, which methylates DNA at the O6 position of guanine, leading to DNA mismatches during replication (Tolcher et al., 2003). The mismatches trigger DNA damage responses and lead to cell cycle arrest and tumour cell apoptosis. The effectiveness of TMZ depends largely on the activity of the DNA repair

enzyme MGMT (O6-methylguanine-DNA methyltransferase): high MGMT expression can repair the damage and cause resistance, while low MGMT levels enhance sensitivity to TMZ treatment (Stupp et al., 2005).

Radiation therapy and TMZ are used as a concomitant therapy in glioblastoma post-surgery, followed by adjuvant temozolomide treatment. Stupp et al. demonstrated increase in patient overall survival with radiation therapy and concomitant/adjuvant TMZ therapy compared to radiation therapy alone: median overall survival 14.6 months vs. 12.1 months (Stupp et al., 2005). Since then, the radiation therapy and concomitant/adjuvant TMZ therapy has been the standard for glioblastoma treatment post-surgery.

1.2.3 Prognosis

The median survival time among glioblastoma patients is 15 months and a 5-year survival is only 7.2% (Ostrom et al., 2023). The major prognostic factors for glioblastoma are age of the patient and MGMT promoter methylation (Brown et al., 2022). Younger patients (< 50-year-olds) have better recovery from surgery, which can be seen in life expectancy. The younger patients are also more likely to receive the standard therapy (surgery and radiation therapy with concomitant and adjuvant temozolomide treatment) for glioblastoma rather than non-standard or no therapy. MGMT promoter methylation indicates better response for TMZ treatment. The promoter methylation represses transcription of the *MGMT* gene and decreases MGMT activity (Stupp et al., 2005).

Tumour location has a significant effect on maximal safe resection in surgery. Patients with tumours located in central brain structures, such as corpus callosum and basal ganglia, and left temporal lobe are reported to have survival of less than 6 months (Fyllingen et al., 2021). Tumours in the dorsomedial right temporal lobe and the white matter region are reported to be associated with much longer survival (> 24 months). The effect of tumour location in glioblastoma survival is not entirely clear, another study has reported that tumour laterality (right or left hemisphere) has no effect on patient survival (Liu et al., 2016).

1.2.4 Glioblastoma heterogeneity

Inter-patient heterogeneity is a significant factor in glioblastoma. Glioblastoma is driven by a broad number of mutations and cell states, and thus every glioblastoma tumour has unique characteristics.

The extensive inter-patient heterogeneity is supported by glioblastoma transcript profiling. Inter-patient heterogeneity in genomic alterations is significant in glioblastoma, but the most common genomic alterations include *TP53, EGFR, PDGFR,* and *PTEN* (Table 2) (Wang et al., 2017). Verhaak et al. (2010) presented four glioblastoma subtypes based on expression profiles of glioblastoma-associated genes. These subtypes were proneural, mesenchymal, classical and neural. However, the glioblastoma subtypes were later redefined into three tumor-intrinsic subtypes (proneural, classical, mesenchymal) when the neural subtype was excluded as it reflected non–tumour (normal neural) contamination (Wang et al., 2017).

Table 2. Glioblastoma molecular subtypes and their characteristic gene expression profiles. Adapted from (Wang et al., 2017).

Subtype	**Key genetic alterations**	**Characteristic gene expression signatures**
Proneural	PDGFRA amplification TP53 mutation	OLIG2 ↑ ASCL1 ↑ SOX ↑ Progenitor-like gene expression
Mesenchymal	NF1 deletion/mutation TP53 mutation PTEN mutation	Nestin ↑ Notch pathway ↑ Progenitor-like gene expression
Classical	EGFR mutation/amplification CKDN2A deletion	CD44 ↑ Mesenchymal transition gene expression TNF/NF-κB signature
Neural (removed)	Gene signature similar to normal brain	Gene signature similar to normal brain

In addition to inter-patient heterogeneity, glioblastoma exhibits profound intra-tumoural heterogeneity. It is shown that spatially distinct biopsies taken from the same tumour harbour substantial genetic variation, including regional differences in key driver alterations such as *EGFR* and *CDKN2A/B* amplifications (Sottoriva et al., 2013). Neftel et al. (2019) have demonstrated that individual glioblastoma tumours contain multiple co-existing cellular states, including neural progenitor cell-like, oligodendrocyte precursor cell-like, astrocyte-like, and mesenchymal-like populations. The states are dynamic, and genetic, epigenetic and microenvironmental factors can cause tumour cells to transition between them (Neftel et al., 2019). These shifts in phenotypic states further enhance intra-tumoural complexity of glioblastoma. The findings have revealed a branched evolutionary pattern within individual tumours, demonstrating that single biopsies often capture only a fraction of the tumour's molecular diversity. The cellular states have multiple effects on glioblastoma phenotype.

Doroszko et al. (2025) have shown that the cellular states of glioblastoma correlate with distinct invasion phenotypes: mesenchymal-like cells exhibit perivascular invasion, whereas neural progenitor cell-like and astrocyte-like cell populations display diffuse invasion in mouse xenografts. It is also reported that the changes in cellular states can cause shifts in glioblastoma invasion phenotypes (Doroszko et al., 2025).

Overall, both inter-patient and intra-tumoural heterogeneity are key factors that complicate therapeutic targeting in glioblastoma, as they result in diverse molecular profiles and functional behaviours within and between tumours.

1.2.5 Glioblastoma cellular origin

The cellular origin of glioblastoma is not fully understood, but two dominant theories have been presented: stem cell theory and dedifferentiation theory. Both these acknowledge the complex heterogeneity of glioblastoma and suggest that multiple cellular routes contribute to development of glioblastoma.

Historically, it was believed that the adult brain lacked regenerative capacity, and that astrocytes were the only glial cells capable of division. However, this view was challenged by discovery of self-renewing and multipotent neural stem cells (NSCs) in the human brain in the 1990s (Obernier & Alvarez-Buylla, 2019). These NSCs are primarily found in the subventricular zone and the hippocampal dentate gyrus (Bond et al., 2015). Notably, many of the gliomas, including glioblastomas, often arise in close proximity to the subventricular zone, suggesting a possible link between NSCs and tumour initiation (Jung et al., 2024).

According to stem cell theory, glioblastoma may originate from neural stem cells or glial progenitor cells, including oligodendrocyte precursor (OPC) and astrocyte precursor (APC) cells, that acquire oncogenic mutations (Sloan et al., 2024). These mutations lead to uncontrolled proliferation, impaired differentiation, and increased invasion capacity (Liu et al., 2011; Sloan et al., 2024). The mutations may occur in relatively undifferentiated cells with high proliferative potential, allowing them to serve as a reservoir for tumour development. Supporting this theory, many glioblastomas exhibit molecular signatures and gene expression similar to those seen in NSCs and progenitor cells, such as *NES* (Nestin), *SOX2*, and *PDGFRα* (Lottaz et al., 2010; Sloan et al., 2024; Suvà et al., 2014).

In contrast, the dedifferentiation theory proposes that glioblastoma can arise when mature, differentiated glial cells, such as astrocytes, undergo genetic or epigenetic changes that cause

them to revert to a more primitive and stem-like state. This process of cellular reprogramming enables these cells to reacquire self-renewal capacity and resist regulatory signals that normally control cell division. There has been evidence that differentiated astrocytes can give rise to glioblastoma-like tumours in mouse models when key tumour suppressor genes (e.g. *TP53*, *PTEN*) are inactivated (Friedmann-Morvinski et al., 2012).

Recent studies suggest that both mechanisms may contribute to glioblastoma development, depending on the subtype of the tumour. Proneural glioblastomas are thought to originate more often from neural stem cells or oligodendrocyte precursor cells, while mesenchymal subtypes may arise from dedifferentiated astrocytes or other glial cells (Verhaak et al., 2010). Spatial transcriptomics and single-cell RNA sequencing have demonstrated that glioblastomas contain a mix of tumour cells in different states: some expressing highly stem-like characteristics and others being more differentiated. It is also speculated that the cells can shift between these states and might explain the treatment resistance and recurrence of glioblastoma (Neftel et al., 2019).

While the exact cellular origin of glioblastoma is not fully resolved, the evidence supports that tumour-initiating cells may arise either from mutated neural stem/progenitor cells or from dedifferentiated mature glia. Understanding the initiating cell type and the early development of glioblastoma remains a critical goal, as it may open new ways for early detection, targeted therapies, and prevention of recurrence.

1.3 Human Glioblastoma Cell Culture

Traditional glioblastoma cell lines, such as U87 and U251, have been widely used in glioblastoma research, but they have several critical limitations. First, when grown in a serum-containing medium, the cells undergo changes that no longer reflect the genetic and molecular features of the tumour of origin (Lee et al., 2006). Glioblastoma cells with stem/progenitor-like characteristics have important functions in glioblastoma tumour initiation and therapy resistance in the disease. Second, the traditional glioblastoma cell lines show poor morphological similarities to glioblastoma tumours when xenografted into the mouse brain (Lee et al., 2006). Lack of diffuse infiltration and microvascular proliferation are histopathological characteristics that are absent in these xenografts. Lastly, the clinical data of the glioblastoma tumours, from where the traditional glioblastoma cell lines originate, is incomplete. The lack of clinical data decreases the translational relevance of research findings in these cell lines (Xie et al., 2015).

In 2015, Xie et al. presented new cell lines for glioblastoma research. The Human Glioblastoma Cell Culture (HGCC) resource (www.hgcc.se) is a publicly available collection of glioblastoma cell lines developed from patient tumour samples in Uppsala University. The HGCC biobank has 48 well-defined and characterised glioblastoma cell lines representing all three transcriptional subtypes of glioblastoma. The cell lines are cultured in serum-free conditions to preserve stem/progenitor-like cell activity and to prevent changes in molecular and genomic characteristics in glioblastoma cells.

The key advantage of HGCC cell cultures is clinical relevance to the origin tumours. Each HGCC cell line is thoroughly characterised through genomic, transcriptomic and clinical profiling increasing the translational relevance of research findings using these cell lines.

1.4 Chick Chorioallantoic Membrane

Chick Chorioallantoic Membrane (CAM) is a valuable alternative *in vivo* model to traditional rodent models in biomedical research, particularly in the fields of oncology, angiogenesis, and drug development (Wang et al., 2025). The CAM model was originally developed as a tool for angiogenesis research, providing a valuable system for studying blood vessel formation in tumours. Over time, its utility has expanded, and it is now recognised as a versatile platform for xenograft studies. This chapter outlines the biological foundation of the CAM model, its development, structure, and unique properties that make it suitable for tumour modelling, including glioblastoma tumours (Fischer et al., 2022).

1.4.1 Development and structure of the CAM

The chorioallantoic membrane develops through the fusion of two extraembryonic membranes: the chorion and the allantois (Nagai et al., 2022). The fusion begins around embryonic development day 3 (EDD 3) and results in the formation of a highly vascularised membrane that lies just beneath the eggshell. By approximately EDD 10, the CAM has expanded to cover the entire inner surface of the eggshell, providing a large, accessible surface suitable for experimental manipulation (Fischer et al., 2022). The timeline of chick development from incubation (EDD 0) to hatching (EDD 21/22) is illustrated in Figure 1.

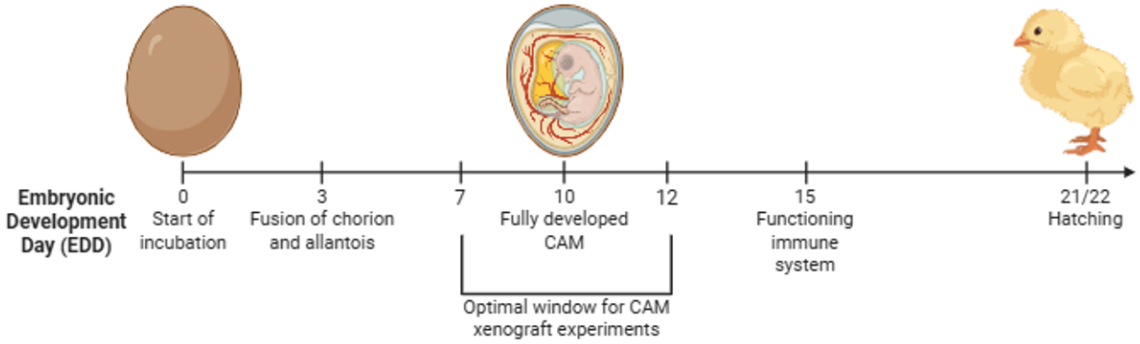

Figure 1. Timeline of chick embryo development. Created with BioRender.com.

Structurally, the CAM is a thin, transparent extraembryonic membrane that plays essential physiological roles in gas exchange, calcium mobilisation from the eggshell, and waste elimination during embryogenesis (Fischer et al., 2022). Under normal conditions, CAM thickness ranges from 20 to 100 µm, although thickening can occur in response to mechanical or environmental stress. The CAM comprises three distinct layers: the ectoderm (chorionic epithelium), the mesoderm, and the endoderm (allantoic epithelium) (Figure 2). The ectoderm forms the outermost epithelial layer immediately beneath the eggshell. The endoderm forms the inner epithelial boundary facing the allantoic cavity. Between these layers is the mesoderm, a stromal layer rich in extracellular matrix, fibroblasts, and a dense vascular network (Nowak-Sliwinska et al., 2014). As highlighted by Fischer et al. (2022), the mesoderm is of particular relevance for tumour biology because its extensive vasculature and strong angiogenic capacity provide a supportive microenvironment for studying tumour-induced angiogenesis and invasion.

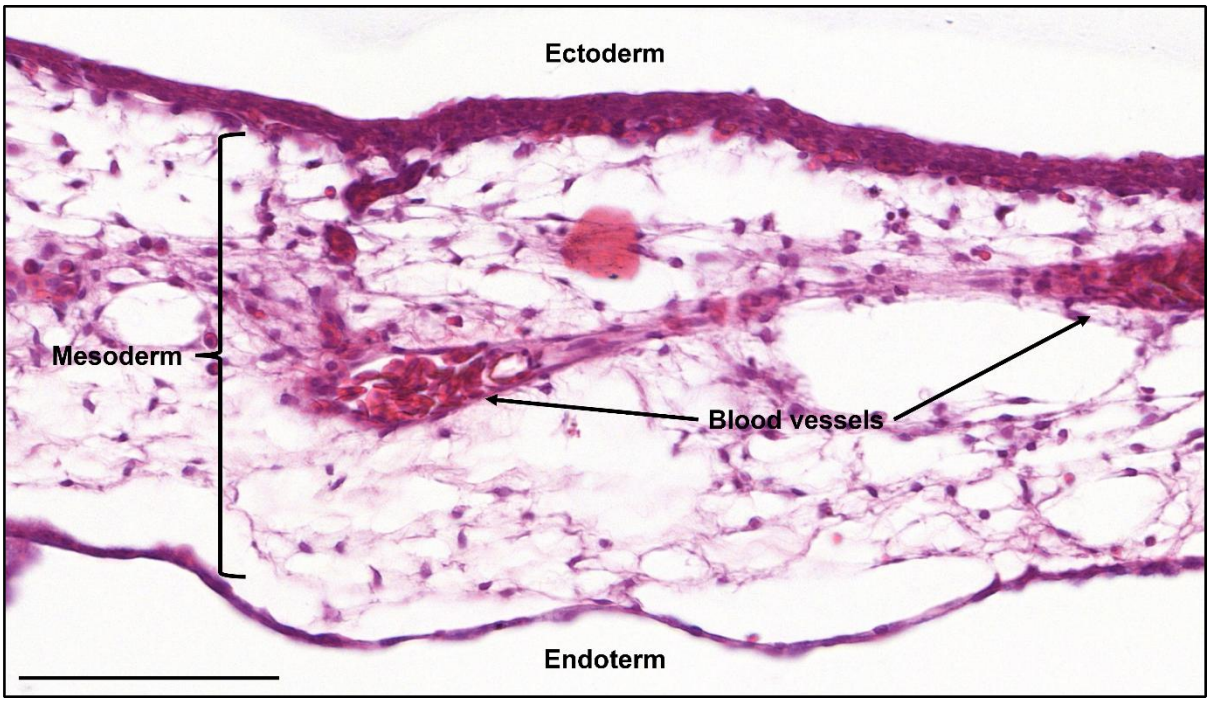

Figure 2. Chorioallantoic membrane structure on embryonic development day 12. Scale bar = 100 µm.

1.4.2 Immune environment of the CAM model

One of the key advantages of the CAM model is its natural immunodeficiency during early embryonic development, which allows successful engraftment of human tumour cells without triggering immune rejection (Fischer et al., 2022). The immune system of the chick embryo develops gradually between EDD 12 and EDD 18. T cells and B cells first appear around EDD 12, whereas a fully functional adaptive immune system is established by approximately EDD 18 (Janse & Jeurissen, 1991). Although the adaptive immune system is immature during early development, innate immune components such as macrophage-like cells are already present in the CAM around EDD 3 – 5 (Fischer et al., 2022). EDD 15 is often considered a critical timepoint after which immune activity may begin to interfere with xenografted tumour cells (Janse & Jeurissen, 1991). The overall immune competence increases with embryonic age, meaning that immune reactivity becomes more pronounced in later stages of development (Fischer et al., 2022).

Although this naturally occurring immunodeficient window is a major advantage for xenograft experiments, it also presents limitations. The absence of mature adaptive immunity means that interactions between tumour cells and immune cells, an essential component of tumour progression and therapeutic response in mammalian systems, are not replicated in the CAM model (Fischer et al., 2022). This also means that immunotherapies cannot be effectively

studied in the CAM model because meaningful interactions between tumour cells and a mature adaptive immune system are absent.

1.4.3 Advantages and limitations of the CAM model in cancer research

The chorioallantoic model serves as a versatile *in vivo* (or *in ovo*) platform that bridges the gap between *in vitro* studies and traditional mammalian *in vivo* models, offering a biologically relevant yet practical system for tumour research (Fischer et al., 2022). It provides several advantages that make it particularly attractive for cancer studies.

Chick embryos are not classified as live animals until later stages of development, and the flexibility of ethical regulations makes the model more accessible. According to the EU Directive 2010/63 on the protection of animals used for scientific purposes, embryonic and foetal forms are likely to experience pain only when their nervous system has sufficiently matured, which occurs after approximately two-thirds of development. For chick embryos, this corresponds to EDD 14. Consequently, CAM experiments conducted and terminated before EDD 14 generally do not require formal ethical approval within the European Union.

In addition to regulatory advantages, the CAM model is inexpensive and requires minimal infrastructure compared to rodent models. Experiments can be performed in a basic laboratory environment, and fertilised eggs are easy to obtain (Meneceur et al., 2020). The external location of xenografts on the CAM enables real-time visualisation of tumour engraftment, vascularisation, and invasion using standard imaging techniques such as fluorescence or bioluminescence imaging (Fischer et al., 2022). These features make the CAM model ideal for large-scale preclinical studies.

A major strength of the CAM model is its rapid experimental timeline. Tumour grafts become vascularised within just a few days, allowing experiments to be completed in 5 – 10 days (Meneceur et al., 2020). Tumour formation occurs significantly faster than in rodent models, where establishing xenografts may take weeks or months (Meneceur et al., 2020). The CAM environment strongly supports tumour cell survival and proliferation, resulting in high engraftment efficiency compared to mammalian models (Meneceur et al., 2020).

Despite its advantages, the CAM model has notable limitations. A key constraint is the lack of a mature immune system, as mentioned above. While early immunodeficiency facilitates xenografting, it restricts the study of immune–tumour interactions and prevents meaningful assessment of immunotherapies (Fischer et al., 2022). The short experimental window limits

studies on long-term tumour progression, treatment effects, and metastasis (Fischer et al., 2022). Additionally, the CAM lacks the complex tissue architecture and microenvironment of human organs. For glioblastoma research specifically, the absence of brain-specific extracellular matrix, neuronal–glial interactions, and blood–brain barrier components reduce the accuracy of tumour–host interactions (Ribatti, 2022). Additionally, pharmacological studies are limited by the embryo's immature drug metabolism, which differs significantly from that of adult mammals (Ribatti, 2014). As a result, drug efficacy, toxicity, and pharmacokinetics observed in the CAM model do not completely translate to mammalian systems.

Overall, while the CAM model offers a powerful, efficient, and accessible platform for studying tumour biology, angiogenesis and treatment effects, its limitations must be recognised when interpreting findings or translating results into mammalian preclinical or clinical contexts. Importantly, the chorioallantoic membrane is an easily accessible *in vivo* model that takes the experiments a step further from *in vitro* studies.

1.5 Ubiquitin proteasome system

The ubiquitin–proteasome system (UPS) is the principal intracellular pathway responsible for selective protein degradation in all eukaryotic cells and is essential for maintaining cellular homeostasis (Roos-Mattjus & Sistonen, 2004). It regulates numerous cellular processes, including cell survival, cell-cycle control, DNA repair, antigen presentation, and apoptosis. Errors in protein synthesis frequently lead to misfolded or damaged proteins, and the UPS is critical for eliminating these aberrant proteins and enabling the recycling of amino acids (Roos-Mattjus & Sistonen, 2004). The UPS also regulates the lifespan of short-lived regulatory proteins, such as cyclins, transcription factors, and signalling mediators, ensuring precise control over cellular pathways. Approximately 80–90% of intracellular protein degradation occurs through this system (Soave et al., 2017).

The UPS functions in two sequential and highly coordinated steps: substrate ubiquitination and proteasomal degradation of the target protein. Ubiquitin is a 76-amino-acid polypeptide that serves as a degradation tag (Damgaard, 2021). Ubiquitination of a substrate protein involves three enzymes: ubiquitin-activating enzyme E1, ubiquitin-conjugating enzyme E2, and ubiquitin ligase E3 (Roos-Mattjus & Sistonen, 2004). First, E1 activates ubiquitin in an ATP-dependent reaction, forming an E1–ubiquitin ester. Activated ubiquitin is transferred to E2, which cooperates with an E3 ligase to recognize the substrate protein. The ubiquitin molecule is then covalently attached to a lysine residue on the substrate. Repeated cycles result in

polyubiquitination, typically through linkage at lysine 48 of ubiquitin. A tetraubiquitin chain is considered the minimal effective signal for proteasomal degradation, with degradation efficiency increasing as more ubiquitin units are added (Thrower et al., 2000).

Polyubiquitinated proteins are recognized and processed by the 26S proteasome, a large ATP-dependent protease located primarily in the cytoplasm. The 26S proteasome consists of a cylindrical 20S core particle and one or two 19S regulatory particles (Roos-Mattjus & Sistonen, 2004). The polyubiquitin chain binds to receptors within the 19S regulatory particle, which unfolds the substrate and removes the ubiquitin molecules for recycling. The unfolded polypeptide is then translocated into the 20S core particle, which contains proteolytic sites that cleave the substrate into oligopeptides of 2–24 amino acids (Saric et al., 2004). These peptides are subsequently degraded by aminopeptidases into free amino acids that can be reused for new protein synthesis.

1.5.1 Ubiquitin proteasome system in cancer

Cancer cells display extensive alterations in UPS activity that support malignant growth. Increased proliferation elevates the need for UPS activation to maintain proteostasis and remove misfolded or damaged proteins when the protein synthesis is accelerated. The activity of several UPS components is frequently dysregulated in cancer cells, and higher proteasome subunit expression and increased proteasome activity have been reported across several cancer types (Arlt et al., 2009; Chen & Madura, 2005). The higher proteasome activity has also been observed in gliomas (He et al., 2024). Many key oncoproteins and tumour suppressors are UPS substrates, including for example tumour suppressors p53, p21, and p27, which play central roles in controlling cell-cycle checkpoints (Park et al., 2020; Vlachostergios et al., 2012).

p53 is one of the most important tumour suppressors regulated by the UPS. Under normal conditions, p53 is kept at low levels through continuous ubiquitination by the E3 ligase MDM2, targeting it for proteasomal degradation (Haupt et al., 1997). In response to cellular stress, such as DNA damage, p53 becomes stabilised and activates transcription of genes involved in cell-cycle arrest, DNA repair, and apoptosis. In many cancers, including glioblastoma, altered UPS activity or MDM2 overexpression leads to excessive p53 degradation, weakening checkpoint control and enabling tumour progression (Park et al., 2020).

p21 contributes to checkpoint control in both G1 and G2 phases. It inhibits Cdk2 during G1 and Cdk1 during G2, helping maintain cell-cycle arrest when necessary. Increased UPS-mediated

degradation of p21 promotes aberrant cell-cycle progression and loss of checkpoint control (Abbas & Dutta, 2009).

p27 functions as a negative regulator of cyclin D–Cdk4, cyclin E–Cdk2, and cyclin A–Cdk2 complexes, thereby regulating the transition from G1 to S phase. Increased proteasome activity leads to reduced p27 protein levels, and p27 is low or almost absent in many high-grade gliomas and glioblastomas (Piva et al., 1999).

Taken together, dysregulated UPS activity in cancer promotes oncogenic signalling, weakens tumour suppressor pathways, enhances proliferation, and enables tumour cells, including glioblastomas, to adapt to elevated proteotoxic stress. These dependencies suggest that glioblastoma cells may be susceptible to treatments that target proteasomal degradation.

1.5.2 Proteasome inhibition with bortezomib

Proteasome inhibitors, such as bortezomib, are a class of drugs that block the enzymatic activity of the 20S core particle within the 26S proteasome. Bortezomib is a boronate peptide that reversibly inhibits the chymotrypsin-like activity of the 20S proteasome subunit (Adams, 2004). It is approved by both the EMA and FDA for the treatment of multiple myeloma and mantle cell lymphoma.

Proteasome inhibitors do not fully block 26S proteasome function: the 19S regulatory particle remains active and continues to recognise, deubiquitinate, and unfold ubiquitin-tagged substrates. Inhibition of the 20S core particle prevents these unfolded proteins from being degraded. As a result, unfolded proteins accumulate in the cytosol and within the endoplasmic reticulum (ER), where they overwhelm normal protein-folding capacity. This accumulation triggers ER stress and activation of an unfolded protein response (UPR), a compensatory pathway aimed at restoring proteostasis (Obeng et al., 2006). If ER stress remains unresolved, UPR signalling shifts from adaptive to pro-apoptotic, contributing to cell death. In addition, bortezomib induces increased levels of reactive oxygen species (ROS), which further promote apoptotic signalling in cancer cells (Chauhan et al., 2005).

A degree of bortezomib effects in cancer cells may be initiated through retained activity of cell-cycle regulators, p21, p27, and p53, as described in the previous chapter. Proteasome impairment has been shown to stabilise p53 and activate stress-response pathways, further contributing to apoptosis (Kruiswijk et al., 2015). Another major mechanism of action in proteasome inhibition with bortezomib is the inhibition of NF-κB signalling. Under normal

conditions, activation of NF-κB requires proteasomal degradation of its inhibitor, IκBα. When bortezomib prevents IκBα degradation, NF-κB remains inactive, reducing transcription of anti-apoptotic and cell-survival genes (Adams, 2004).

In summary, several mechanisms may contribute to the effects of bortezomib in glioblastoma cells. Proteasome inhibition leads to the accumulation of unfolded proteins, triggering ER stress and activating the unfolded protein response (Obeng et al., 2006). Prolonged stress promotes apoptosis, which is further enhanced by increased ROS generation (Chauhan et al., 2005). Stabilization of key UPS-regulated tumour suppressors such as p53 can amplify pro-apoptotic signalling, demonstrating that proteasome inhibition can lead to p53 accumulation and stress-induced cell death (Kruiswijk et al., 2015). Bortezomib also suppresses NF-κB signalling by stabilizing IκBα, reducing transcription of survival and anti-apoptotic genes (Adams, 2004). Although the exact mechanism of action of bortezomib in glioblastoma cells is not completely understood, these pathways suggest that sensitivity to bortezomib is a combination of proteotoxic stress, oxidative stress responses, and regained activity of apoptotic and cell-cycle regulatory mechanisms.

2 RESULTS

2.1 Validation of CAM model for glioblastoma growth and invasion

2.1.1 Glioblastoma tumour formation and invasion in CAM model

The first aim of this thesis project was to study growth of glioblastoma cell lines in the CAM model. A total of 17 HGCC cell lines were xenografted onto the chorioallantoic membrane of fertilised chicken eggs. These cell lines represented all glioblastoma subtypes – proneural, classical, and mesenchymal (Table 3). Xenografts from each cell line were divided into two timepoints for tumour collection and analysis: Day 3 and Day 5 after cell inoculation. The take-out rate, indicating the percentage of xenografts that successfully formed tumours, was calculated for each cell line to assess reproducibility of tumour formation in the model. All the 17 cell lines showed successful tumour formation, with an average take-out rate exceeding 90% and ranging from 78% to 100% between cell lines. These results demonstrate that the CAM model provides a highly supportive environment for glioblastoma xenografting.

Table 3. Glioblastoma cell lines for tumour growth and invasion experiment.

Cell line	Subtype	Take-out rate	Replicates (*n*) (Day 3, Day 5)
U3005	Proneural	100%	9 (4, 5)
U3008	Classical	100%	26 (15, 11)
U3013	Proneural	95%	18 (9, 9)
U3017	Classical	80%	16 (9, 7)
U3047	Proneural	100%	18 (9, 9)
U3051	Classical	96%	23 (12, 11)
U3054	Mesenchymal	90%	18 (9, 9)
U3065	Proneural	90%	27 (14, 13)
U3118	Proneural	100%	22 (11, 11)
U3137	Mesenchymal	87%	18 (5, 13)
U3173	Mesenchymal	82%	18 (7, 11)
U3179	Classical	92%	11 (4, 7)
U3180	Classical	100%	12 (6, 6)
U3202	Mesenchymal	78%	12 (6, 6)
U3213	Mesenchymal	86%	19 (9, 10)
U3220	Mesenchymal	95%	17 (9, 8)
U3230	Classical	80%	16 (8, 8)

The tumours from all cell lines were photographed and harvested for histological analysis. Hematoxylin and eosin (HE) staining and immunohistochemistry (IHC) using Stem121, a marker for human cytoplasmic proteins, was done to analyse tumour formation and invasion (Figure 3). Distinct morphological differences were observed between glioblastoma cell lines: some xenografts formed topical and bulgy tumours (Figure 3A, J), while others exhibited flat and evenly spread growths (Figure 3G) that were often difficult to detect macroscopically but clearly visible in histological sections. A subset of xenografts developed tumours deeper within the chorioallantoic membrane (Figure 3D). No consistent tumour formation pattern was associated with any specific glioblastoma subtype. Stem121 IHC staining confirmed that the tumour masses observed in HE staining originated from human glioblastoma cells (Figure 3C, F, I, L).

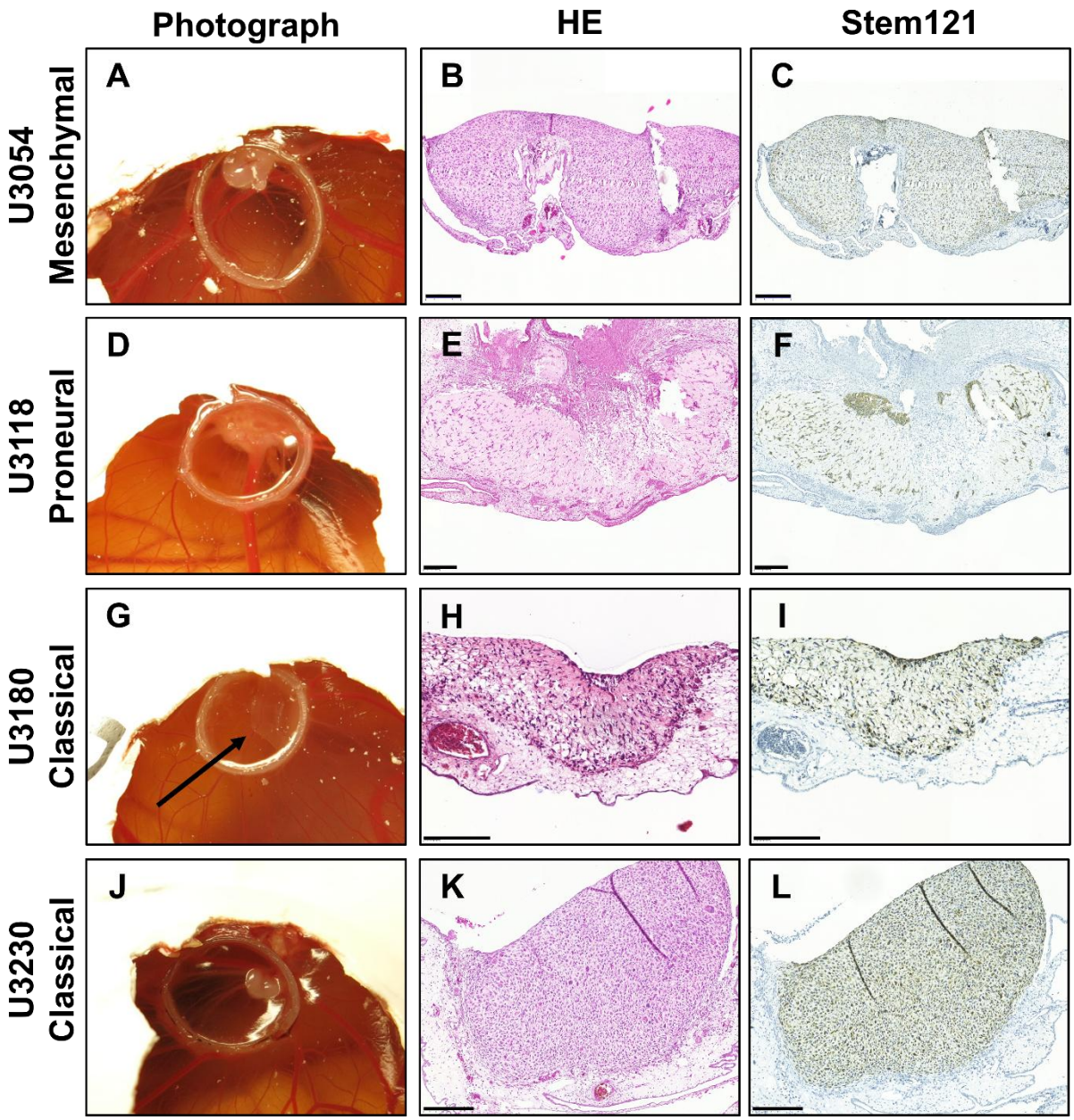

Figure 3. Representative glioblastoma tumour formation and invasion in CAM xenografts. HGCC cell lines from all subtypes: U3054 **(A–C)**, U3118 **(D–F)**, U3180 (**G-I)**, U3230 **(J–L)**. Tumours displayed variable morphology, including topical and bulgy formations **(A, J)**, deep intramembranous growths **(D)**, and flat, evenly spread tumours **(G, arrow).** HE staining revealed different levels of CAM invasion **(B, E, H, K)**, and Stem121 immunostaining confirmed the human tumour cell origin **(C, F, I, L)**. Scale bars = 200 µm.

The tumour invasion of the CAM was further examined by histological analysis. HE staining revealed varying degrees of tumour penetration into the CAM, which was classified on a 3-way scale: high, moderate, or low invasion. Intact CAM structure consists of three layers: the ectoderm (outer epithelial layer), the mesoderm (vascular stroma), and the endoderm (inner epithelial layer) (Figure 2). The high invasion tumours infiltrated the ectoderm and most of the mesoderm, leaving only the bottom layer of the membrane (endoderm) intact (Figure 4A).

Tumours with moderate invasion reached a substantial portion of the mesoderm, but the bottom half of the CAM remained intact (Figure 4B). The low invasion tumours only slightly infiltrated the ectoderm or the whole membrane stayed intact (Figure 4C). Additionally, some xenografts formed tumours entirely within the CAM (Figure 4D), where an irregularly shaped ectoderm was observed above the tumour mass. Variation in invasion patterns was clear between cell lines, but no subtype-specific trends were identified.

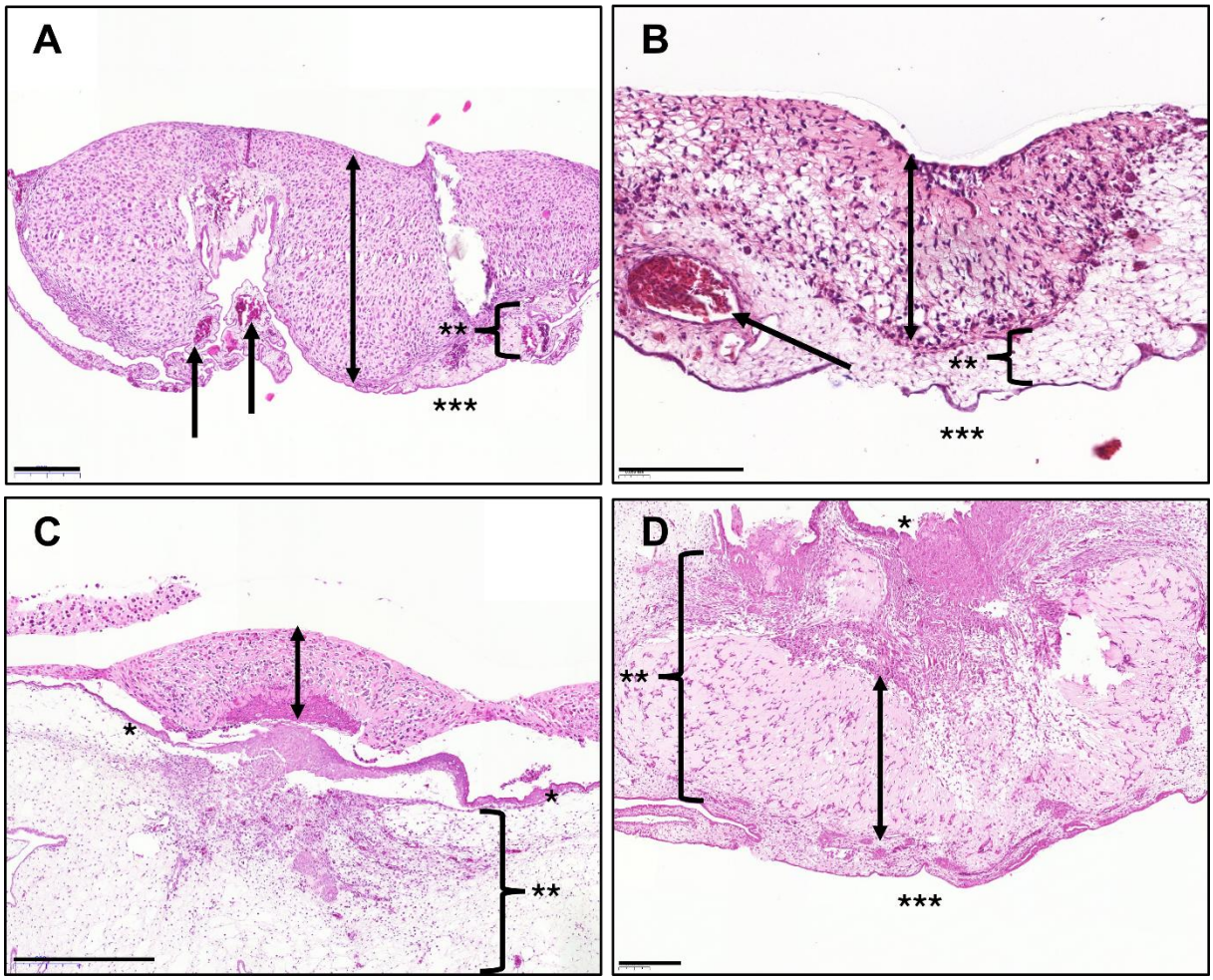

Figure 4. Levels of glioblastoma tumour invasion into chorioallantoic membrane. HE staining of four xenografts with different invasion levels: U3054 Mesenchymal with high invasion **(A)**, U3180 Classical with moderate invasion **(B)**, U3005 Proneural with low invasion **(C)**, and U3118 Proneural with deep intramembranous growth **(D)**. Structural layers of the membrane and tumour mass are annotated: ectoderm (*), mesoderm (**), endoderm (***), blood vessels (arrow), and tumour mass (double-headed arrow). Scale bars = 200 µm.

Chorioallantoic membrane hyperplasia was consistently observed in glioblastoma xenografts. The hyperplasia was characterised by an expansion of the mesodermal layer below the tumour implantation site. Even though the CAM thickening was not always significant, some

xenografts showed extreme CAM hyperplasia where the membrane thickness exceeded the size of the tumour (Figure 5).

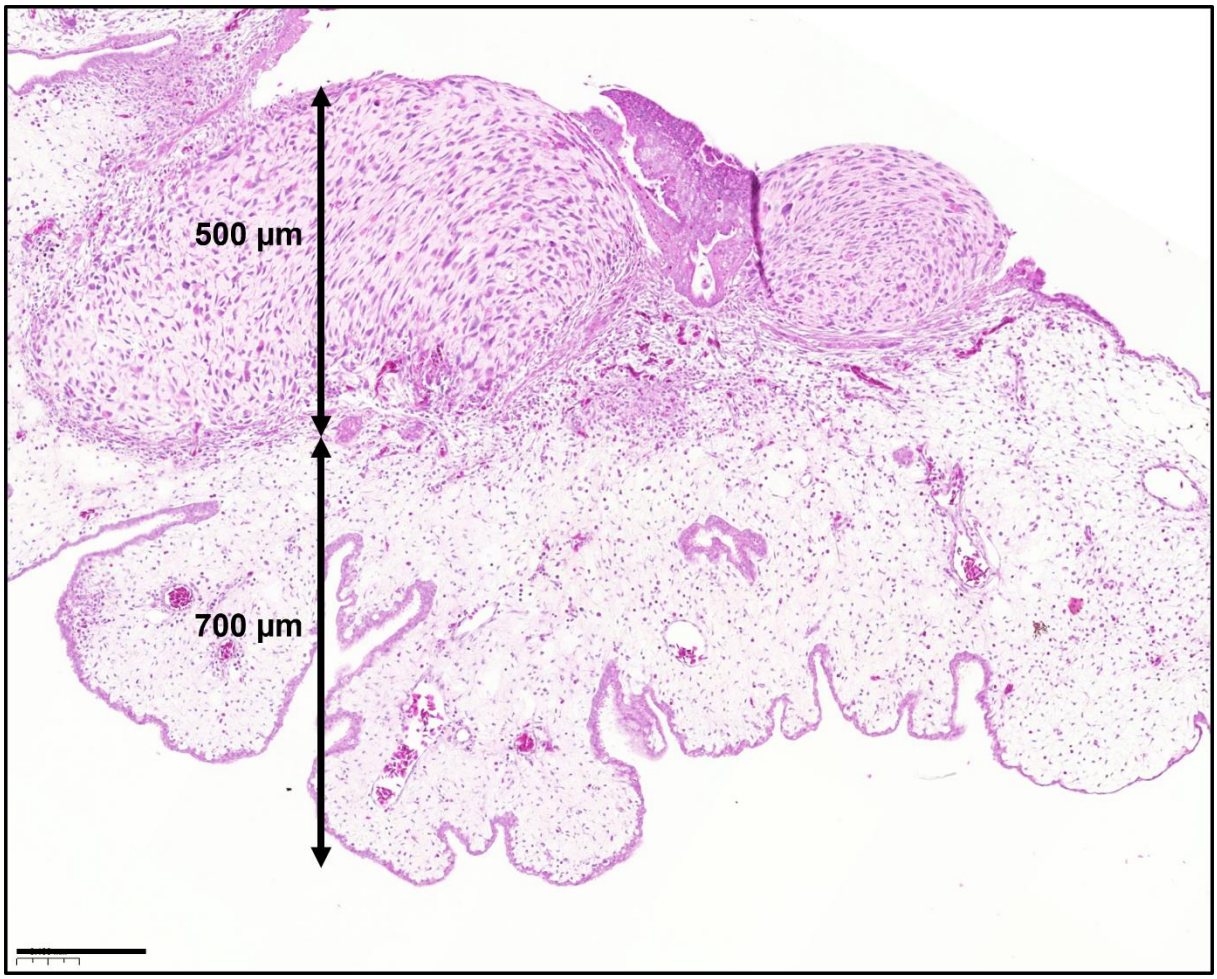

Figure 5. Chorioallantoic membrane hyperplasia under stress. Representative image showing HE staining of U3065 tumour (top double-headed arrow) and associated thickening of the underlying CAM tissue (bottom double-headed arrow). Scale bar = 200 µm.

2.1.2 Vascularisation of the CAM in glioblastoma xenografts

High vasculature of the CAM is one of the key characteristics of the model and the membrane becomes increasingly vascularised during progression of the embryonic development. The vascularisation of CAM in xenografts was identified by IHC using Von Willebran Factor (vWF) antibody (Figure 6). The IHC staining using vWF antibody was conducted for xenografts of 15 glioblastoma cell lines, U3005 and U3179 xenografts were not analysed with vWF immunostaining.

Vascularisation was clearly visible on the embryonic development day 10 (Figure 6A). Smaller capillaries were seen in HE staining of the xenograft (Figure 6B) and these capillaries formed

in the lower part of the mesoderm. IHC analysis using vWF was done to further highlight the location of vasculature in the CAM (Figure 6C, D). The capillary network was identified to form close to the tumour and some microvasculature was seen on the edge of the tumour (Figure 6D, leftmost arrow). The vascularisation of the CAM was consistent in all analysed xenografts, but vascularisation reaching inside of the tumour mass was not observed.

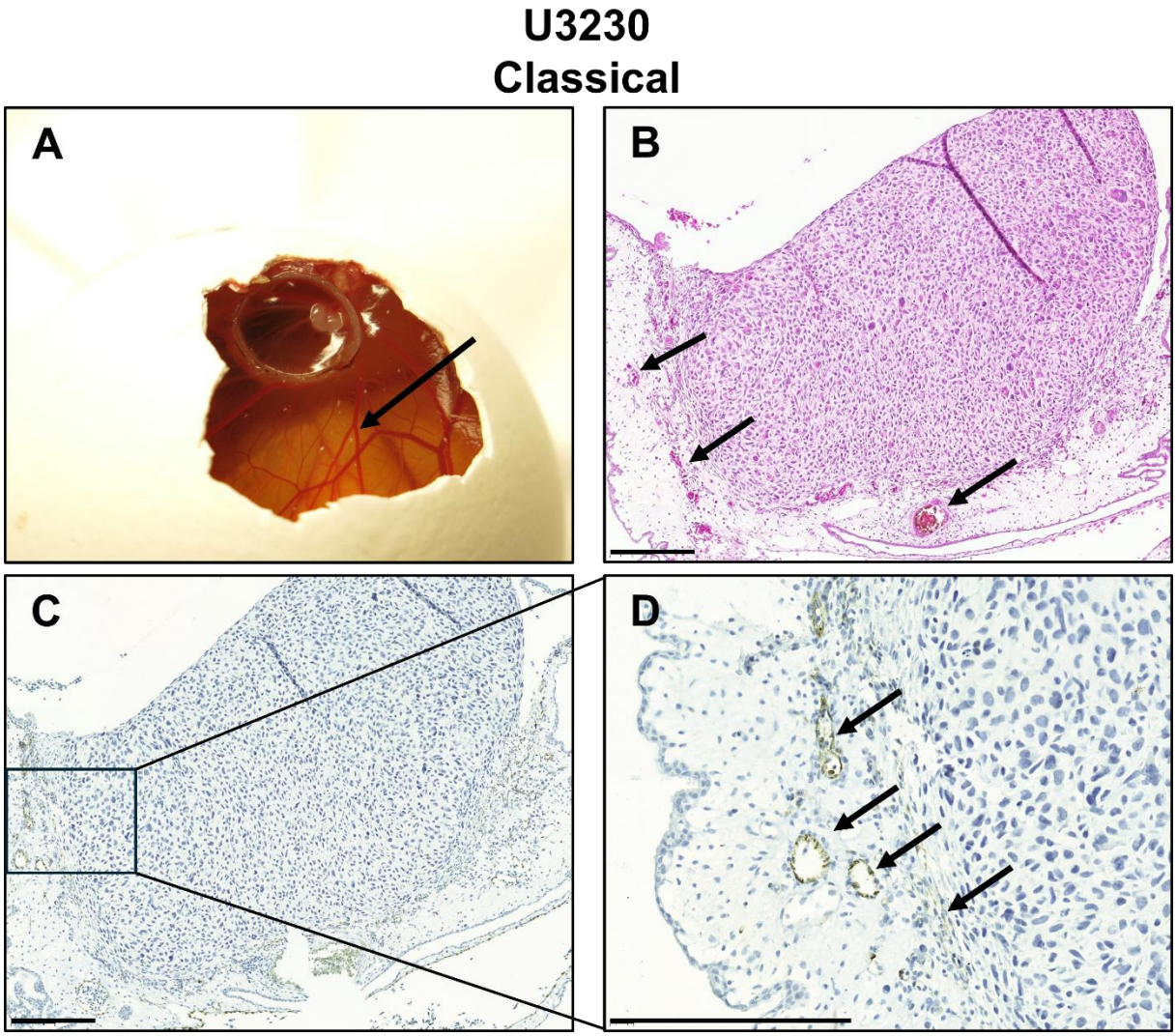

Figure 6. Representative vascularisation of the chorioallantoic membrane around glioblastoma tumour. The figure presents vascularisation in U3230 (Classical) xenograft. The vascularisation was clearly visible in photograph of the tumour **(A, arrow)**. The smaller capillaries were visible in HE staining **(B, arrows)**. IHC using vWF marker highlighted the capillaries close to the tumour **(C, D)**. Microvasculature was seen on the edge of the tumour **(D, arrows)**. Scale bars = 200μm.

2.1.3 Tumour growth assessment by tumour weight

The growth of the tumours over time was analysed by comparing weights of the tumours dissected at two timepoints: three days (Day 3) and five days (Day 5) after inoculation. The change in tumour weight over time was analysed by comparing the weights (mean) of the two groups. Statistical significance was calculated using unpaired Welch's t-test or Mann-Whitney test. Statistically significant tumour growth ($p < 0.05$) was observed in six of the 17 cell lines (Table 4, green). Two of the cell lines showed statistically significant decrease ($p < 0.05$) in tumour weight (Table 4, red). The remaining nine cell lines did not have significant change in tumour weight (Table 4, yellow).

Table 4. Glioblastoma tumour weight change in CAM xenografts from Day 3 to Day 5.

Cell line	Subtype	Replicates (*n*) (Day 3, Day 5)	Tumour weight change Day 3 vs. Day 5 (mg)	*p* value
U3005	Proneural	9 (4, 5)	**-23,0**	***p* < 0.01 ****
U3008	Classical	26 (15, 11)	**9,3**	***p* < 0.05 ***
U3013	Proneural	18 (9, 9)	**11,8**	***p* < 0.05 ***
U3017	Classical	16 (9, 7)	10,8	*p* > 0.05
U3047	Proneural	18 (9, 9)	-8,1	*p* > 0.05
U3051	Classical	23 (12, 11)	**15,3**	***p* < 0.01 ****
U3054	Mesenchymal	18 (9, 9)	**20,0**	***p* < 0.001 *****
U3065	Proneural	27 (14, 13)	-8,2	*p* > 0.05
U3118	Proneural	22 (11, 11)	0,5	*p* > 0.05
U3137	Mesenchymal	18 (5, 13)	**-9,4**	***p* < 0.05 ***
U3173	Mesenchymal	18 (7, 11)	**11,1**	***p* < 0.05 ***
U3179	Classical	11 (4, 7)	-13,4	*p* > 0.05
U3180	Classical	12 (6, 6)	**13,3**	***p* < 0.05 ***
U3202	Mesenchymal	12 (6, 6)	0,9	*p* > 0.05
U3213	Mesenchymal	19 (9, 10)	8,6	*p* > 0.05
U3220	Mesenchymal	17 (9, 8)	-1,1	*p* > 0.05
U3230	Classical	16 (8, 8)	10,3	*p* > 0.05

All glioblastoma subtypes showed both increase and no change in tumour weights, indicating that growth progression is not dependent of the subtype (Figure 7). The cell lines U3008 ($p < 0.05$), U3054 ($p < 0.001$) and U3013 ($p < 0.05$) showed statistically significant increase in tumour weight. The cell lines U3017, U3213 and U3047 did not show statistically significant

change in tumour weight. Many cell lines showed notable variation in tumour weights within groups: for example, U3017 showed higher tumour weight with increased variation in Day 5 group compared to Day 3 group, indicating that the growth of tumours is not consistent within a cell line (Figure 7). Complete tumour weight data for all 17 cell lines can be seen in Appendix 1.

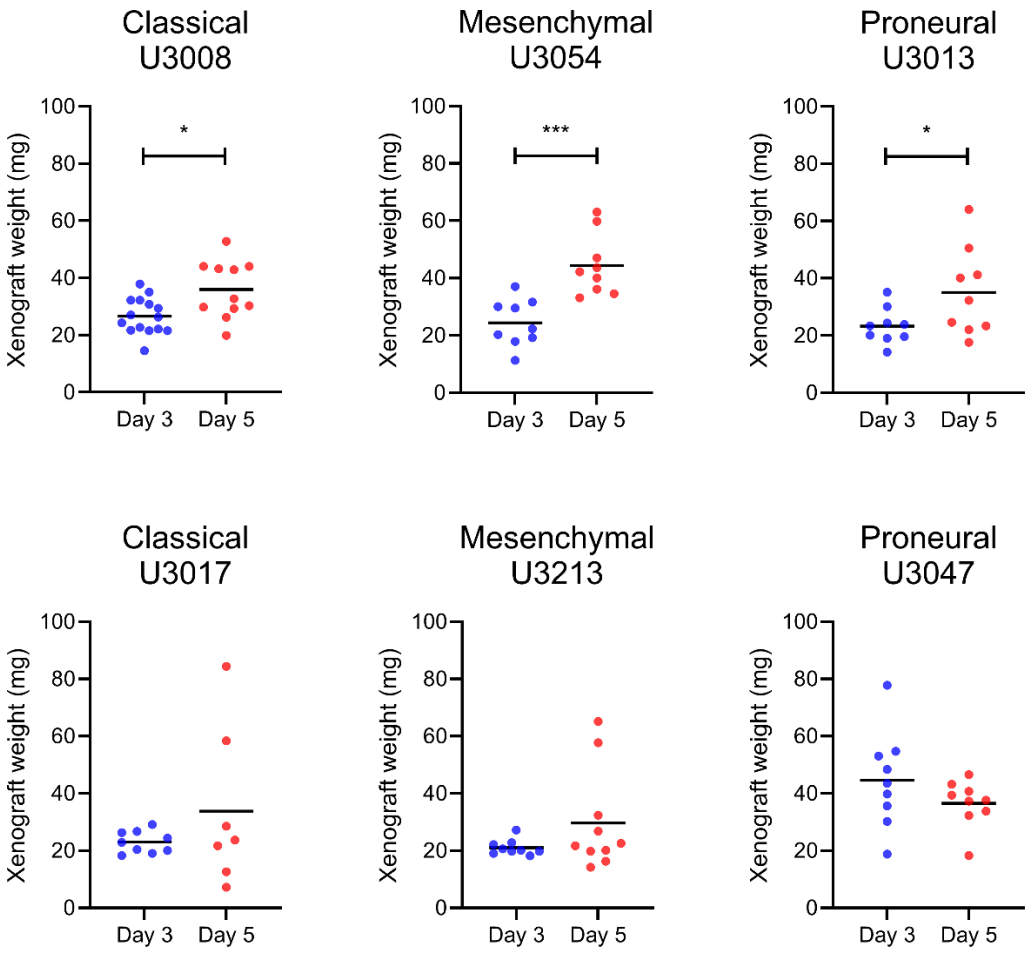

Figure 7. Representative graphs of tumour weights in glioblastoma xenografts. Statistically significant increase in tumour weights (top row) and no significant change (bottom row) was seen in all glioblastoma subtypes. Statistical significance: $p < 0.05$ *, $p < 0.01$ **, $p < 0.001$ ***.

2.1.4 Glioblastoma cell proliferation in the CAM xenografts

Since dissected xenografts include both the CAM and glioblastoma components, the weight alone can be a confounding parameter to analyse tumour growth. Immunohistochemistry with

human anti-Ki67 proliferation marker was used to evaluate glioblastoma proliferation in the CAM model. All 17 cell lines showed Ki67-positive tumour cells, confirming that active proliferation was present in all of them. Ki67 expression showed variation in proliferation rates between cell lines (Table 5). The proliferation rate of the tumours was classified as high (+++: Ki67-index > 30%), moderate (++: Ki67-index = 15 – 30%), or low (+: Ki67-index < 15%). U3008, U3013, U3051, U3054, U3173, and U3220 xenografts showed the highest proliferation rates, whereas the lowest proliferation rates were observed in U3047, U3179, and U3202 xenografts. Even though differences in proliferation rates were observed between cell lines, variation in Ki67 expression was also present in tumours of the same cell line.

Table 5. Glioblastoma cell proliferation rates in CAM xenografts.

Cell line	Subtype	Ki67-positive cells
U3005	Proneural	++
U3008	Classical	+++
U3013	Proneural	+++
U3017	Classical	++
U3047	Proneural	+
U3051	Classical	+++
U3054	Mesenchymal	+++
U3065	Proneural	++
U3118	Proneural	++

Cell line	Subtype	Ki67-positive cells
U3137	Mesenchymal	++
U3173	Mesenchymal	+++
U3179	Classical	+
U3180	Classical	++
U3202	Mesenchymal	+
U3213	Mesenchymal	++
U3220	Mesenchymal	+++
U3230	Classical	++

Representative images of Ki67 signals in the xenografts are shown in Figure 8. The U3013 cell line showed a high number of Ki67-positive cells (Figure 8A, B), indicating high proliferation rate, whereas the U3017 cell line showed moderate proliferation (Figure 8C and D). In contrast, the U3202 cell line showed low Ki67 expression (Figure 8E and F), indicating reduced proliferation compared to U3013 and U3017 cell lines.

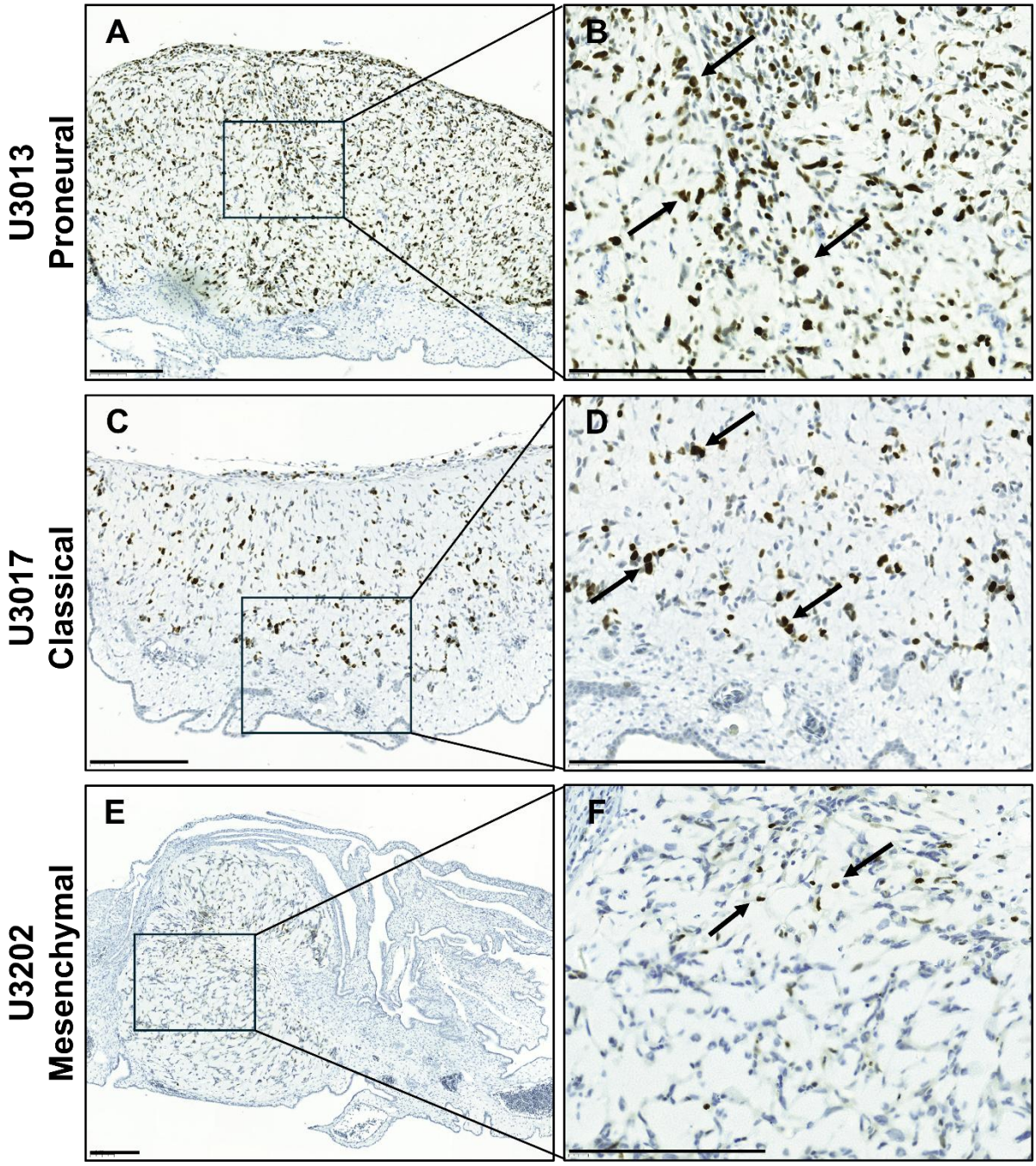

Figure 8. Glioblastoma cell proliferation in CAM xenografts. Representative images of anti-Ki67 IHC staining of three xenograft tumours: U3013 tumour with high number of Ki67 positive cells **(A, B)**, U3017 tumour with moderate number Ki67 positive cells **(C, D)**, and U3202 tumour with low number of Ki67 positive cells **(E, F)**. Scale bars = 200 µm.

2.1.5 Evaluation of cancer stem cells in CAM xenografts

Stem cell-like and progenitor cell-like properties of the glioblastoma cells are thought to be the driving force behind aggressiveness of the disease. The HGCC cell lines used in this experiment retain stem/progenitor-like properties *in vitro*. To confirm that these properties were retained *in vivo*, immunohistochemistry using a Nestin stem/progenitor cell marker was performed on the

xenografts. All 17 glioblastoma cell lines displayed clear Nestin positivity in the xenografts, indicating that stem/progenitor cell-like properties were preserved within the CAM model. Representative images of IHC using anti-Nestin are shown in Figure 9: high Nestin expression was observed in U3118, U3180, and U3220 xenografts.

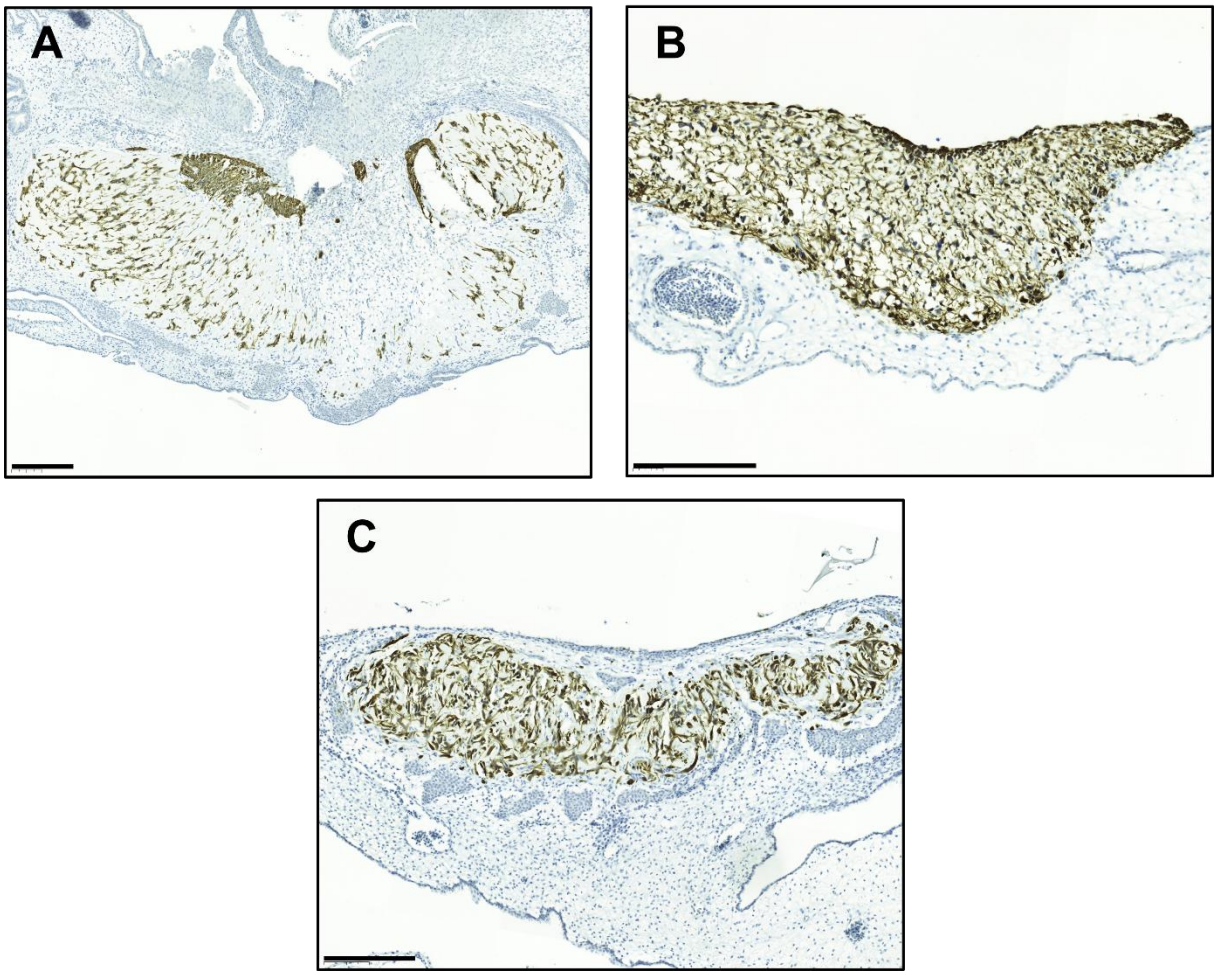

Figure 9. Stem/progenitor-like cell expression in CAM xenografts. Nestin IHC staining of three xenografts: **(A)** U3118 (Proneural), **(B)** U3180 (Classical), and **(C)** U3220 (Mesenchymal). All tumours showed clear Nestin positivity, confirming retention of stem/progenitor-like characteristics in xenografts. Scale bars = 200 µm.

2.2 Validation of CAM model for testing glioblastoma treatment

The second aim of this thesis was to investigate the suitability of the CAM model for glioblastoma treatment studies. Drug screening and *in vitro* studies of Nelander lab have demonstrated that certain glioblastoma cell cultures express sensitivity to proteasome inhibitors. Thus, the treatment experiment was conducted using proteasome inhibitor bortezomib in concentrations of 5 µg/kg (BTZ5) and 10 µg/kg (BTZ10). A total of nine GFP-Luc -labelled glioblastoma cell lines were selected for this experiment: four cell lines with

mesenchymal subtype, four cell lines with classical subtype, and one cell line with proneural subtype (Table 6). The xenografts of each cell line were divided into three groups: control, BTZ5, and BTZ10. Only two groups, control and BTZ10, were used for the U3179 cell line due to the limited number of surviving embryos. The changes in tumour growth and glioblastoma cell viability were monitored using bioluminescence imaging (BLI). Baseline BLI signals were measured on Day 3 (three days after xenografting), and the treatment was applied topically on the tumours. BLI signal was measured again on Day 5, and the relative change in BLI signal intensity was calculated for each xenograft. Statistical analysis was performed for each glioblastoma cell line to compare the treatment groups against untreated controls.

Table 6. Glioblastoma cell lines for treatment experiment.

Cell line	Replicates (*n*) (Control, BTZ5, BTZ10)	Relative BLI signal (Day 5 – Day 3)			*p* value Control vs. BTZ5	*p* value Control vs. BTZ10
		Control (Mean ±SD)	BTZ5 (Mean ±SD)	BTZ10 (Mean ±SD)		
U3008	(12, 11, 11)	$-1.41 \times 10^{8} \pm 4.17 \times 10^{8}$	$-1.94 \times 10^{8} \pm 3.26 \times 10^{8}$	$-1.53 \times 10^{8} \pm 4.33 \times 10^{8}$	$p > 0.05$	$p > 0.05$
U3013	(10, 11, 10)	$3.27 \times 10^{8} \pm 4.17 \times 10^{8}$	$-3.18 \times 10^{8} \pm 4.28 \times 10^{8}$	$-4.07 \times 10^{8} \pm 5.39 \times 10^{8}$	$p < 0.01$ **	$p < 0.01$ **
U3017	(18, 4, 18)	$4.77 \times 10^{7} \pm 5.32 \times 10^{7}$	$-8.39 \times 10^{6} \pm 5.50 \times 10^{7}$	$-5.53 \times 10^{7} \pm 4.75 \times 10^{7}$	$p > 0.05$	$p < 0.0001$ ****
U3054	(13, 11, 12)	$5.59 \times 10^{8} \pm 2.60 \times 10^{8}$	$-1.84 \times 10^{8} \pm 4.36 \times 10^{8}$	$-5.00 \times 10^{8} \pm 4.59 \times 10^{8}$	$p < 0.01$ **	$p < 0.0001$ ****
U3137	(15, 6, 9)	$2.04 \times 10^{7} \pm 2.22 \times 10^{7}$	$1.69 \times 10^{7} \pm 1.14 \times 10^{7}$	$-7.40 \times 10^{6} \pm 2.27 \times 10^{7}$	$p > 0.05$	$p < 0.01$ **
U3173	(11, 7, 9)	$-1.65 \times 10^{11} \pm 1.50 \times 10^{11}$	$-6.37 \times 10^{10} \pm 9.08 \times 10^{10}$	$-1.10 \times 10^{11} \pm 9.87 \times 10^{10}$	$p > 0.05$	$p > 0.05$
U3179	(12, 0, 10)	$5.82 \times 10^{7} \pm 8.25 \times 10^{7}$		$-1.02 \times 10^{8} \pm 1.02 \times 10^{8}$		$p < 0.001$ ***
U3180	(17, 13, 19)	$5.95 \times 10^{7} \pm 3.13 \times 10^{8}$	$2.35 \times 10^{8} \pm 4.02 \times 10^{8}$	$1.35 \times 10^{8} \pm 3.76 \times 10^{8}$	$p > 0.05$	$p > 0.05$
U3213	(10, 8, 10)	$-9.66 \times 10^{10} \pm 9.08 \times 10^{10}$	$-6.42 \times 10^{10} \pm 6.28 \times 10^{10}$	$-7.95 \times 10^{10} \pm 5.87 \times 10^{10}$	$p > 0.05$	$p > 0.05$

Five out of the nine glioblastoma cell lines showed sensitivity to bortezomib (Table 6, green), while the remaining four cell lines did not show detectable effect for bortezomib treatment (Table 6, red). Two of the five sensitive cell lines showed statistically significant effect for both bortezomib concentrations (U3013 and U3054), while two cell lines showed statistically

significant effect only for higher concentration (U3017 and U3137). U3179 with only one treatment group showed statistically significant effect for the higher bortezomib concentration.

Mesenchymal and classical subtypes showed both sensitivity and no effect for bortezomib treatment, indicating that there was no specific treatment effect for either subtype. The one cell line with proneural subtype (U3013) showed sensitivity for the treatment (Table 6).

Figure 10 presents the relative change of BLI signal in xenografts from five cell lines. Three of these cell lines showed sensitivity for bortezomib treatment (U3017, U3054, and U3013), while two cell lines did not show any detectable effect (U3008 and U3213). U3054 and U3013 cell lines showed statistically significant effect for both bortezomib concentrations. U3017 showed statistically significant sensitivity for the higher bortezomib concentration, while weaker effect was observed in the lower concentration.

Complete BLI data for all glioblastoma cell lines used in the treatment experiment can be seen in Appendix 2.

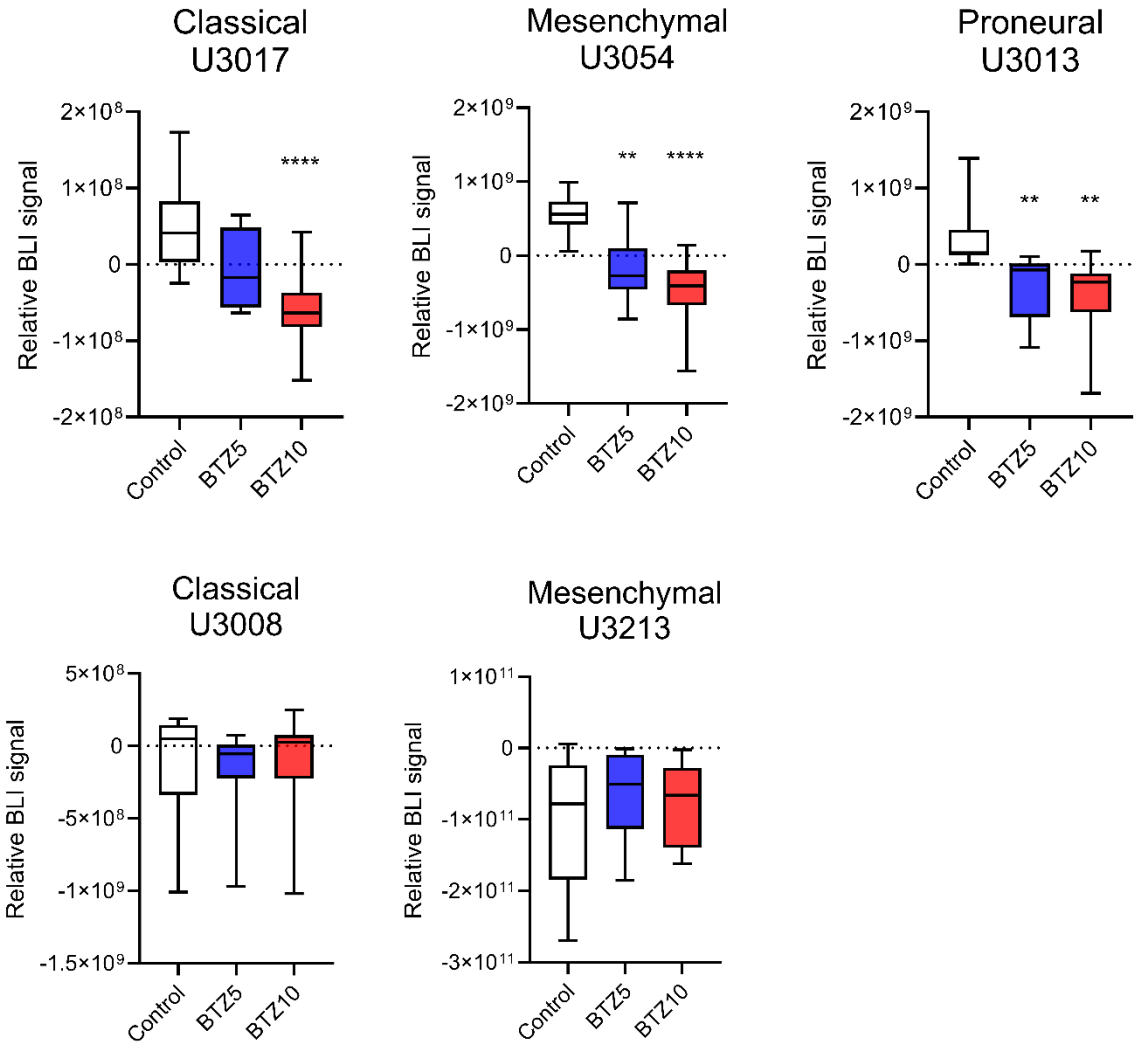

Figure 10. Relative change in BLI signal in xenografts of five glioblastoma cell lines. U3017, U3054, and U3013 xenografts showed clear sensitivity for bortezomib treatment. Resistance for bortezomib treatment was observed in U3008 and U3213 xenografts. Statistical significance: $p < 0.05$ *, $p < 0.01$ **, $p < 0.001$ ***, $p < 0.0001$ ****.

3 DISCUSSION

The chick chorioallantoic membrane model has gained attention as a cost-efficient and versatile *in vivo* model for preclinical studies. In this study, the CAM model was used to investigate glioblastoma growth, invasion, and response to proteasome inhibition using a panel of patient-derived HGCC cell lines, representing all transcriptional subtypes of glioblastoma. The main objectives were to validate suitability of the CAM model for glioblastoma xenografting and investigate its potential for drug treatment screening. The results of this study demonstrate that the CAM model provides a rapid and relatively reproducible system for glioblastoma tumour growth, invasion, and treatment – with certain limitations.

3.1 Characterisation of glioblastoma xenografts in the CAM model

The first notable result of this study was that all the 17 glioblastoma cell lines showed successful tumour formation in the CAM model with high tumour takeout rates (78 – 100%, average > 90%). The high success rate in tumour formation demonstrates that the CAM, with its growth factors and nutrients, provides a supportive microenvironment for glioblastoma xenografting. In comparison, a recent study of xenografting HGCC cells into mouse brain reported successful tumour formation only in 28 out of 43 cell lines (Krona et al., 2025). The tumour development also required significantly longer time, with latency periods ranging from less than 50 days to over 200 days, depending on the aggressiveness of the cell line. Slower glioblastoma tumour formation and lower success rate has also been reported in other rodent studies (Meneceur et al., 2020). These results highlight the efficiency and reliability of the CAM model for glioblastoma tumour development.

Macroscopic and histological evaluation revealed substantial heterogeneity in tumour morphology and invasion among the glioblastoma xenografts. The implanted glioblastoma cell lines formed both bulgy/elevated tumours and flat/diffusely spread tumours. The same differences in tumour morphology have been observed in rodent xenografts (Krona et al., 2025). Additionally, certain cell lines consistently expressed deep intramembranous tumour growths, where the tumour mass appeared deep within the CAM layers. These intramembranous tumours were clearly visible both macroscopically and in histological analysis.

The underlying cause of these intramembranous growths remains unclear. One possible explanation is that highly invasive glioblastoma cells actively migrated into the mesoderm shortly after xenografting, seeking a more nutrient- and oxygen-rich environment around the

blood vessels. Alternatively, technical factors may contribute to this phenotype. If the CAM surface was disrupted during cell inoculation, the tumour cells could gain early access inside the membrane and proliferate there. Moreover, the orientation of histological samples could also influence the apparent tumour position, particularly if the sections are taken at a non-perpendicular angle. Even though the technical factors need to be considered, the consistency of intramembranous growths within certain cell lines supports the idea that these are accurate invasion phenotypes and not due to technical errors.

Invasion analysis based on HE staining revealed that glioblastoma cells could penetrate deep into the CAM and differences in depth of the invasion was clearly seen between cell lines. No consistent correlation between glioblastoma subtype and tumour morphology or invasion pattern was detected. Inter-patient and intra-tumoural heterogeneity are well known characteristics in glioblastoma (Eisenbarth & Wang, 2023), and this translates to patient-derived glioblastoma cell lines. Similar heterogeneity in HGCC glioblastoma tumour invasion has been observed in studies with mouse xenografts (Doroszko et al., 2025; Krona et al., 2025). Diversity in growth patterns of the cell lines used in this study was clearly seen *in vitro* while culturing cells. This highlights how each glioblastoma cell line needs to be analysed individually: the unique mutation profile and molecular characteristics of the cell line lead to distinct features seen in tumour morphology and invasion. Diversity in morphology and invasion was also detected within cell lines, indicating that environmental factors or technical errors in conducting experiments might have an effect. Additional research is needed to fully distinguish the tumour morphology and invasion pattern of each glioblastoma cell line. Despite the differences in morphology and invasion, the observed tumour formation in the xenografts suggest that the CAM model provides a biologically relevant environment for studying early stages of glioblastoma growth and invasion.

Confirmation of human tumour origin by Stem121 staining ensured that the observed growth originated from the implanted glioblastoma cells. This validation is crucial in mixed-species models, where distinguishing human tumour tissue from host cells can be difficult. Strong Stem121 signal was observed in all cell lines, and this staining highly reflected the assumed tumour mass seen in HE staining. The most important aspect in Stem121 staining was to distinguish glioblastoma tumour mass from CAM hyperplasia. Morphological changes and hyperplasia of the CAM are common stress response in the model (DeBord et al., 2018), and these were clearly seen in the glioblastoma xenografts.

Hyperplasia of the chorioallantoic membrane was seen in most of the xenografts. The immune system of the CAM model develops gradually and starts functioning around EDD 10 – 12 (Fischer et al., 2022). Even though the immune system does not reject the xenograft in the early stages, it can cause a non-specific immune response (Ribatti, 2022). It has also been reported that functional macrophages can trigger an immune response in the CAM already around EDD 9 (Dhayer et al., 2024). The observed CAM hyperplasia is likely a consequence of early immune responses triggered by glioblastoma xenografts.

Vascularisation is a defining feature of glioblastoma and a key factor supporting its aggressiveness by providing nutrients and oxygen. In this study, the vascular network was observed to be centralised around the tumour site in macroscopical evaluation of the tumour photographs. In addition, von Willebrand factor staining revealed a high density of blood vessels surrounding the tumours, with microcapillaries often extending towards the edge of the tumour. Vascularisation was not observed inside the tumours. The CAM vascularisation increases fast in early stages of embryonic development, and it forms an extraordinarily dense network of vessels in the mesoderm of the membrane (Nowak-Sliwinska et al., 2014). Presence of blood vessels in the CAM may attract glioblastoma cells and cause them to migrate towards oxygen and nutrient rich environment. This migration of glioblastoma cells towards blood vessels inside the CAM is supported by Ribatti (2022). Another reason for blood vessel location in the proximity of the tumour can be that glioblastoma cells secrete pro-angiogenic factors, such as VEGF, which stimulate the formation of blood vessels around the tumour. This idea is supported by centralisation of the blood vessels around tumour site and presence of microcapillaries at the tumour edge, indicating that the tumour microenvironment promotes angiogenesis in the surrounding CAM tissue. Similar observations have been done in other studies (Wang et al., 2025). The absence of vascularisation inside the glioblastoma tumours is likely due to the short duration of the CAM experiments. It can be hypothesised that increased vascularisation around the tumours and even vessel formation inside the tumour would be seen if the experiment could be continued longer.

Presence of glioblastoma stem/progenitor-like cells is thought to be the one of the most important characteristics behind aggressiveness, resistance to therapy, and recurrence of the disease. The used HGCC cell lines are cultured in serum-free medium to retain these characteristics in the cells (Xie et al., 2015). Nestin staining was used to evaluate that the glioblastoma cell lines retained stem/progenitor-like characteristics in the CAM xenografts. Nestin, a marker of neural progenitor and cancer stem cells, is commonly expressed in

glioblastoma (Wang et al., 2021). Nestin expression was consistent in all xenografts, indicating that the stem-like features of the HGCC cell lines were maintained in the CAM xenografts. Comparison of Nestin and Stem121 expression concluded that presence of stem/progenitor-like cells was homogenous in the whole tumour. Presence of stem/progenitor-like cells was crucial for this study and Nestin expression indicates that the CAM xenografts still effectively capture the clinical phenotype of glioblastoma.

Tumour growth, assessed by weight measurements between days three and five, revealed substantial variation among cell lines. Six cell lines showed significant increases in tumour weight, while two displayed weight reduction. The remaining nine cell lines did not show significant change in tumour weight. This variation can be explained by varying proliferation capacities in the cell lines. As discussed above, each glioblastoma cell line must be analysed individually due to unique biological properties. Significant variation in proliferation of the cell lines was also observed *in vitro*, and this translates to the CAM xenografts.

Tumour weight measurement is a common method for evaluating tumour growth progression, but it has clear limitations. Most importantly, the tumour weights at Day 3 and Day 5 represent weights of individual xenografts rather than weight measurements of the same tumour. This introduces undesirable variability to the analysis and does not accurately capture the true tumour growth progression. Possible technical variations in the xenografting process, such as variations in the number of inoculated cells, can have significant impact on tumour development and weight. Furthermore, not all inoculated glioblastoma cells start proliferating with the same efficiency and contribute to tumour development, even within the same cell line, adding variability to tumour growth outcomes. In addition, the weight measurement does not consider the possible necrosis or apoptotic cell death in the tumour, and the CAM hyperplasia can cover a significant amount of the xenograft mass. The results of this study suggest that weight measurement can be an additional tool to evaluate tumour growth, but the results are indicative. Other methods, such as bioluminescence imaging or histological analysis, can give more accurate data of the exact tumour growth, and these methods should be prioritised over tumour weight measurements. Use of bioluminescence imaging to analyse tumour growth progression in this study was not possible due to the limited number of GFP-Luciferase -labelled HGCC cell lines.

Proliferation of the glioblastoma cells in the CAM xenografts was further studied using Ki67 immunostaining, which confirmed proliferative activity across all xenografts. The number of

Ki67-positive cells varied between cell lines, mirroring the heterogeneity observed *in vitro*. Similar differences in Ki67 expression have been reported in HGCC mouse xenografts (Krona et al., 2025). Overall, this variation in proliferation reflects the glioblastoma heterogeneity seen in clinics. Dahlrot et al. (2021) have reported significant variation in Ki67 index (from 0% to over 70%) between glioblastoma patients, with median Ki67 index of 24.4%. Distinct growth progression or proliferation rate was not detected in glioblastoma cell lines with the same subtype, further highlighting that the phenotype is not subtype dependent. Variation in Ki67 expression was also observed in xenografts from the same cell line. This indicates that environmental factors and xenografting procedure can affect glioblastoma cell proliferation in the CAM xenografts. The HGCC cell lines are more sensitive for environmental changes than traditional immortalised glioblastoma cell lines, and this may disturb the proliferation of these cells in the CAM xenografts. A qualitative analysis was conducted to distinguish high, moderate or low proliferation in the cell lines. These results were indicative of the proliferation rate of the cell line, but additional research is needed to robustly connect the degree of proliferation to each cell line. This should be done by quantitative analysis, like Ki67-positive cells counting or other methods to measure Ki67 expression. The quantitative analysis of the Ki67 signal was not possible in the timeframe of this experiment.

3.2 Glioblastoma treatment screening in the CAM model

The response to bortezomib treatment varied significantly between glioblastoma cell lines. Five out of nine tested cell lines showed significant decrease in BLI signal following treatment, indicating reduced cellular viability. The remaining four cell lines showed resistance for the treatment. This heterogenous response reflects the variable clinical sensitivity of glioblastoma for different treatments. No clear relationship between glioblastoma subtype and treatment response was detected, indicating that the subtype alone is insufficient for predicting therapeutic efficacy. The clinical relevance of glioblastoma subtypes has been increasingly questioned by many scientists (Neftel et al., 2019; Verhaak et al., 2010). Neftel et al. (2019) have shown that due to intra-tumoural heterogeneity, individual glioblastoma tumours often contain multiple coexisting cellular programs and can transition between subtypes under stress from treatments. This idea is further supported by the findings of Doroszko et al. (2025).

Bortezomib inhibits the 26S proteasome, leading to accumulation of misfolded proteins, ER stress, and activation of apoptotic pathways. Cancer cells with high proteasome activity or metabolic stress are more dependent on this pathway and thus more sensitive to proteasome

inhibition. The variability in response observed in this study may rise from differences in proteasome dependence, oxidative stress response, or unfolded protein response regulation across the glioblastoma cell lines. The ubiquitin proteasome pathway is a complex and multilayered pathway that has numerous effects inside the cell. The effects how proteasome inhibition leads to death of cancer cells is not fully understood.

The experiments conducted in this thesis were part of a larger study of the Nelander group (Uppsala University), which focused on precision targeting of glioblastoma using patient-derived cell models (Johansson et al., 2020). The data of the treatment experiment was included in that publication as part of the integrated analysis of drug sensitivity. The glioblastoma tumour responses to bortezomib treatment in the CAM model observed in this thesis reflected the results Johansson et al. (2020) saw in *in vitro* studies and *in vivo* mouse studies. Johansson et al. (2020) identified p53 activity and *CDKN2A/B* gene aberrations as possible predictors for treatment response with bortezomib. It is also noted that the current glioblastoma subtypes are insufficient predictors of bortezomib treatment response and use of other optimally selected transcriptional or genetic markers is proposed (Johansson et al., 2020).

Variation in tumour growth and proliferation observed in the growth experiment must be considered when analysing the results of the bortezomib treatment and discussing the CAM model's suitability for drug response screening in glioblastoma. Many glioblastoma cell lines showed variance in tumour growth and proliferation capacity between xenografts. Although not directly observed in this study, it is possible that glioblastoma cell proliferation changes over time in the CAM xenografts. All these can significantly affect the accuracy and interpretation of treatment data. The variations in growth and proliferation may influence the treatment response seen in the experiment by obscuring or exaggerating bortezomib effects. The treatment groups were compared to their corresponding control groups to minimise these impacts, but it cannot completely eliminate the effects of variability. A larger sample size in future experiments is recommended to eliminate the effects of variation in tumour growth and proliferation capacity. Additional research is needed to evaluate how CAM xenografting affects tumour growth and proliferation capacity of glioblastoma cells over time, and how these factors may impact drug response experiments.

3.3 Conclusions

In conclusion, this thesis study presents a CAM model for Human Glioblastoma Cell Cultures that enables glioblastoma tumour growth studies and treatment testing. In addition, the results

of this study support the use of the CAM model as an *in ovo* proxy system for assessing treatment efficacy against glioblastoma tumours. This study demonstrates several key advantages of the chick chorioallantoic membrane model for glioblastoma research. The CAM enables rapid and reproducible tumour formation in a cost-efficient and ethically accessible way. Its short experimental timeline allows efficient screening of multiple glioblastoma cell lines and drug treatments within days, making it an excellent intermediary between *in vitro* assays and preclinical mammalian models. In this study, the CAM model supported tumour growth across all tested HGCC cell lines and reflected the typical heterogeneity of glioblastoma, including features such as proliferation, invasion, and the presence of stem/progenitor-like cells. These characteristics validate the CAM as a feasible short-term *in vivo* platform for studying tumour biology and treatment responses.

However, several limitations must be acknowledged. The CAM lacks the complex neural microenvironment of the human brain, including key components of the extracellular matrix and neuro-glial interactions that shape tumour invasion and treatment response. The absence of a functional immune system prevents investigation of immune–tumour interactions and immunotherapy responses, while the short experimental window restricts studies of long-term tumour evolution, vascularisation, and sustained treatment effects. Importantly, this study revealed considerable variation in tumour growth and treatment response across xenografts, which may complicate the interpretation of treatment efficacy in broad drug screening applications. Factors such as variable tumour initiation, differences in growth progression, and technical variability during xenografting may cause inconsistency to the data. Larger sample size should be used in future experiments to mitigate these effects.

The CAM model is a potential intermediate platform for large-scale drug screening, but additional research and optimisation of the model are required. The advantages of the model, such as efficient tumour formation and short experimental timeline, make it well suited for patient-specific treatment testing. Implanting tumour material or patient-derived glioblastoma cells onto the CAM could allow rapid evaluation of individual treatment responses and offer a path towards making personalised treatment decisions. Further optimisation and validation are required before clinical implementation, but the CAM model shows promise as a complementary tool in the development of personalised treatment strategies against glioblastoma.

4 MATERIALS AND METHODS

4.1 Cell Culture

Glioblastoma cell lines with stem cell-like activity were acquired from Human Glioblastoma Cell Culture resource (Uppsala University, Uppsala, Sweden). The cell lines were selected based on their important characteristics such as aggressiveness of growth, invasiveness, neoangiogenesis and location of origin tumor. Nine of the selected cell lines are publicly available in HGCC resource whereas eight cell lines are currently available only for the Nelander lab. These cell lines represent all glioblastoma subtypes (Table 7). A subset of the cell lines was labelled with GFP and Luciferase. All cell lines were cultured in Primaria T-25 and T-75 flasks (#08-772-45, #08-772-46, Fisher Scientific, Waltham, MA, USA) in serum-free neural stem cell (NSC) media consisting 1:1 mix of DMEM/F12, GlutaMAX (#10565018, Fisher Scientific) and Neurobasal Medium (#21103049, Fisher Scientific) with 1X B-27 (#12587001, Fisher Scientific) and 1X N-2 (#17502001, Fisher Scientific) supplements, 1% Penicillin-Streptomycin (#P4333, Sigma-Aldrich, Saint Louis, MO, USA), 10 ng/mL bFGF (#100-18B, Peprotech, Rocky Hill, NJ, USA) and 10 ng/mL EGF (#AF-100-15, Peprotech). Primaria T-25 and T-75 flasks were coated with 1% laminin (#L2020, Sigma-Aldrich) in sterile PBS at 37°C with 5% CO_2 for at least 1 hour. Detachment of all cell lines was done using StemPro Accutase (#A1110501, Fisher Scientific).

Table 7. Glioblastoma cell lines and their respective subtypes.

Cell line	Subtype	Growth and invasion experiment	Treatment experiment
U3005	Proneural	X	
U3008	Classical	X	X
U3013	Proneural	X	X
U3017	Classical	X	X
U3047	Proneural	X	
U3051	Classical	X	
U3054	Mesenchymal	X	X
U3065	Proneural	X	
U3118	Proneural	X	
U3137	Mesenchymal	X	X
U3173	Mesenchymal	X	X
U3179	Classical	X	X
U3180	Classical	X	X
U3202	Mesenchymal	X	
U3213	Mesenchymal	X	X
U3220	Mesenchymal	X	
U3230	Classical	X	

4.2 Glioblastoma growth and invasion experiment

Experiment timeline for glioblastoma tumour growth and invasion in CAM model is presented in Figure 11. Fertilised White Leghorn chicken eggs were obtained from a local provider (LSK Poultry Oy, Laitila, Finland) within a week after laying. On EDD 0, the eggs were placed upside down into the MG140/200 Rurale incubator (FIEM, Guanzate, Italy) to maintain the right position of vessels and embryo and incubated at 37°C temperature with 60% humidity. On EDD 3, eggshells were pierced using a 20G needle to release pressure inside the eggs and let the CAM settle down. The pierced holes were covered with tape. On EDD 7, the holes were enlarged with forceps and plastic rings were placed on the CAM membrane. A total volume of 20µl of $1x10^6$ glioblastoma cells in 50% Matrigel™ (#11543550, Fisher Scientific) -PBS suspension was applied carefully inside the plastic ring without any contact to the CAM. The xenografts of each cell line were divided into two groups: Day 3 and Day 5. A total of 17 glioblastoma cell lines were used in the growth and invasion experiment (Table 7).

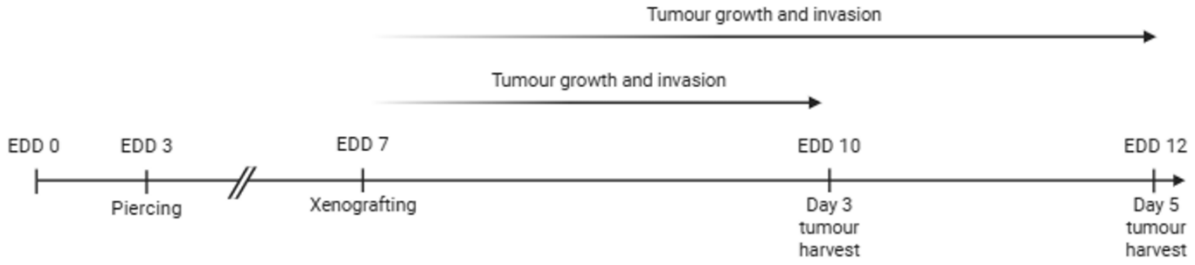

Figure 11. Timeline of glioblastoma tumour growth and invasion experiment in CAM model. Created with BioRender.com.

On EDD 10, the tumours of Day 3 groups were photographed using PowerShot G15 camera (Canon, Tokyo, Japan). After photographing the embryos were sacrificed by placing the eggs on ice for 15 minutes. The xenografts were harvested, and excessive CAM tissue was cleaned from the samples with forceps and scissors. The tumours were weighed with ES 220A scale (#360-9238-001, Precisa, Dietikon, Switzerland). The samples were fixed in 4% phosphate-buffered paraformaldehyde solution (PFA, #30525-89-4, Santa Cruz, Dallas, TX) overnight at 4°C. Same procedure was conducted for tumours of Day 5 groups on EDD 12.

No ethical permit or license was required from the Finnish Animal Ethics Committee to perform this experiment when the embryos were sacrificed before EDD 14.

4.3 Glioblastoma treatment experiment

Timeline for glioblastoma treatment experiment is presented in Figure 12. Fertilised White Leghorn chicken eggs were placed upside down into the MG140/200 Rurale incubator and incubated at 37°C temperature with 60% humidity. Eggshells were pierced on EDD 3 with a 20G needle, and the holes were covered with tape. On EDD 7, the holes were enlarged, plastic rings were placed on the CAM, and a volume of 20µl of $1x10^6$ glioblastoma cells in 50% Matrigel™ - PBS suspension was applied carefully inside the plastic ring without any contact to the CAM. Nine glioblastoma GFP-Luc -labelled cell lines used in the treatment experiment are presented in Table 7. The xenografts of each glioblastoma cell line were divided into three groups: control group and two treatment groups. Proteasome inhibitor bortezomib (PS-341, # S1013, Selleckchem, TX, USA) was used as a treatment compound in two different concentrations: 5 µg/kg (BTZ5) and 10 µg/kg (BTZ10). The 10 µg/kg was determined as the highest non-toxic bortezomib dose.

On EDD 10, 30 µl of a 30 mg/ml luciferin (#LUCNA-250, Zellbio, Ulm, Germany) was applied on the top of the xenografts and IVIS Spectrum camera (PerkinElmer, Shelton, CT, USA) was used to measure baseline bioluminescent signals from Day 3 xenografts. The IVIS imaging sequences and parameters are presented in Appendix 3. After the BLI measurements, the bortezomib treatments were applied topically on the xenografts of corresponding groups. Bortezomib was dissolved to sterile PBS, and the correct treatment volume was calculated from egg weights. Vehicle (0.01% DMSO) was applied to the control groups. The xenografts were incubated for two days after the treatment administration, and the BLI signal of the xenografts was measured again on EDD 12. After the BLI measurement the embryos were sacrificed by placing the eggs on ice for 15 minutes. The xenografts were harvested, weighed and fixed in 4% PFA overnight at 4°C. The BLI signal data was analysed using Living Image 3.2.0 (PerkinElmer) software and data was presented as a difference in BLI signal between Day 3 (EDD 10) and Day 5 (EDD 12).

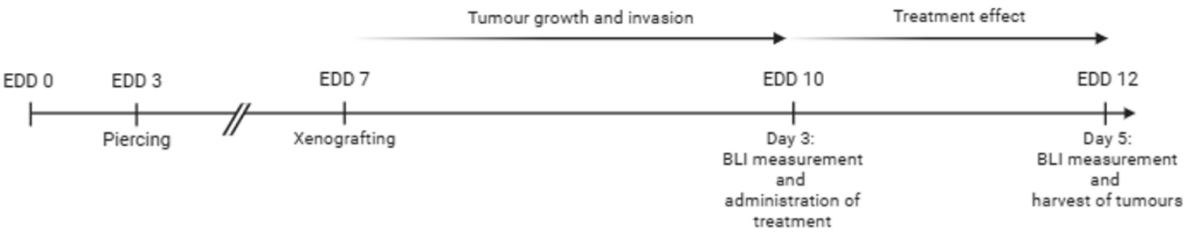

Figure 12. Timeline of glioblastoma treatment experiment in CAM model. Created with BioRender.com.

No ethical permit or license was required from the Finnish Animal Ethics Committee to perform this experiment when the embryos were sacrificed before EDD 14.

4.4 Histology

4.4.1 Processing of histology samples

PFA fixed samples were dehydrated in increasing concentrations of alcohol (70-100%) and embedded into 3% agarose-PBS solution to maintain original orientation of the xenograft for paraffin embedding. Paraffin embedded samples were sectioned into 5 µm slides by using Leica RM2125 RT microtome (Leica Biosystems, Wetzlar, Germany) and mounted on Superfrost plus microscope slides (#10149870, Fisher Scientific, Waltham, MA, USA). The mounted tissue sections were allowed to dry overnight at room temperature. Deparaffinisation and

rehydration were done using xylene and alcohol gradient: xylene (3 x 3 minutes), absolute ethanol (2 x 3 minutes), 96% ethanol (2 x 3 minutes), 70% ethanol (2 x 3 minutes) and deionised water (2 x 5 minutes).

4.4.2 Hematoxylin and Eosin staining

Hematoxylin and eosin (HE) staining was conducted to analyse tumour range in sectioned slides. Slides were stained in Delafield hematoxylin (#01820, HistoLab Products Ab, Askim, Sweden) for 10 minutes, rinsed with tap water, and excess staining was removed using 1% acid alcohol solution (1% HCl in 70% ethanol) for 1 minute. The slides were stained in Eosin (#01650, HistoLab Products Ab) for 2 minutes. Dehydration was conducted with alcohol gradient and xylene: 96% ethanol (1 x 1 minute), absolute ethanol (2 x 1 minute), xylene (2 x 2 minutes). The slides were mounted with Pertex (#00801, HistoLab Products Ab).

4.4.3 Immunohistochemistry

Immunohistochemistry was used to analyse protein expression and localisation of these proteins in the xenografts. Antigens were retrieved using 2100 Antigen Retriever (Aptum Biologics Ltd., Southampton, UK) in Tris-EDTA (pH 9) or citrate buffer (pH 6). TBS with 0.1% Tween20 (#P1379, Sigma-Alrich, Saint Louis, MO, USA) was used as a washing buffer (TBST) and quenching of endogenous peroxidase was done by 10-minute incubation at RT with 3% H_2O_2 in TBS. 3% BSA in TBST for 1 hour at RT was used as a blocking solution. Anti-KI67 MIB-1 (#M7240, Dako, 1:500 dilution), anti-STEM121 (#Y40410, Takara Bio Inc., Kusatsu, Japan, 1:1000 dilution), anti-Nestin (#MA1-110, Invitrogen, Waltham, MA, USA, 1:50 dilution), and anti-vWF (#ab778, Abcam Limited, Cambridge, United Kingdom, 1:30 dilution) diluted in antibody diluent (#BD09-500, Immunologic, Amsterdam, Netherlands) were added on the slides and incubated overnight at 4°C. Sections were incubated with HRP Polymer secondary antibodies anti-rabbit (#DPVR110HRP, Immunologic, Amsterdam, Netherlands) or anti-mouse (#DPVM110HRP, Immunologic, Amsterdam, Netherlands). Bright DAB (3,3'Diaminobenzidine, #BS04-110, Immunologic, Amsterdam, Netherlands) was used as a chromogenic substrate. Sections were counterstained for 20 seconds in Mayer's hematoxylin (#01820, Histolab Products Ab). Dehydration and mounting were done as described above (4.4.2).

4.4.4 Histology slide scanning

Slides were scanned using Pannoramic 250 Slide Scanner (3DHISTECH Ltd., Budapest, Hungary) and Pannoramic Viewer (3DHISTECH Ltd.) was used to take images from the slides.

4.4.5 Qualitative analysis of proliferation rates

Proliferation rates of glioblastoma xenograft tumours were assessed using immunohistochemical staining for Ki67. For each of the 17 glioblastoma cell lines included in this study, Ki67 expression of three independent Day 3 xenograft tumours were analysed.

Proliferation rates were evaluated qualitatively by estimating the proportion of Ki67-positive nuclei within each xenograft. The approximate percentage of Ki67-positive cells was determined based on visual assessment. This analysis was an approximate indicator of proliferative activity rather than an exact quantitative measurement.

Based on the estimated Ki67 indexes, the tumours of each cell line were assigned to one of three proliferation rates: high > 30% (+++), moderate = 15 – 30% (++), or low < 15% (+).

This classification reflects a general proliferative trend and does not represent a statistically validated proliferation rate.

4.5 Statistical analysis

4.5.1 Tumour weight data

Tumour weight data was analysed separately for each 17 cell lines to compare growth between Day 3 and Day 5 groups. All analyses were done using GraphPad Prism (version 10).

Normality of the data in each group was analysed using the Shapiro-Wilk test. If normal distribution was shown in both Day 3 and Day 5 groups, statistical analysis was done using an unpaired Welch's t-test. The unpaired Welch's t-test was chosen over unpaired t-test because of unequal sample size and variance between groups. If at least one group deviated from normality, Mann-Whitney test was used for the statistical analysis. Statistical significance thresholds were defined as $p < 0.05$ (*), $p < 0.01$ (**), and $p < 0.001$ (***).

4.5.2 Bioluminescence data

Treatment effects on tumour growth were assessed by comparing the relative change in bioluminescence (ΔBLI = BLI_Day 5 – BLI_Day 3) between groups (Control, BTZ5, and BTZ10) within each cell line.

For cell lines with three groups, an ordinary one-way ANOVA was used when the data met assumptions of normality and equal variances. When data did not meet the assumptions of normality and equal variances, the Kruskal-Wallis test was used as a nonparametric alternative. One cell line in the treatment experiment had two groups instead of three: control and BTZ10. The statistical analysis for this data was done using an unpaired t-test.

Post-hoc pairwise comparisons were done to analyse control vs. BTZ5 and control vs. BTZ10. The post-hoc comparisons following ANOVA were conducted using Dunnett's test, while the post-hoc comparisons following Kruskal-Wallis were conducted using Dunn's test with adjustment for multiple comparisons.

Statistical significance thresholds were defined as $p < 0.05$ (*), $p < 0.01$ (**), $p < 0.001$ (***), and $p < 0.0001$ (****).

5 ACKNOWLEDGEMENTS

First, I would like to express my deepest gratitude to my supervisors, Milena Doroszko and Petra Sipilä, whose guidance and patience helped me to finish this thesis.

I want to thank you, Milena, for this opportunity and for all the trust you placed in me during this project. I truly admire your work ethic and enthusiasm, and I am grateful for all the things I have learned from you. Your guidance has played an important role in my growth, and I feel fortunate to have worked under your supervision.

Thank you, Petra, for the many ways you have supported me during the last ten years. Much of what I know about scientific research comes from the experiences I gained while working in TCDM and in your research group. It has always been a pleasure to work under your guidance, and I am grateful for those opportunities.

I would like to thank Professor Sven Nelander and the whole Nelander lab, whose work made it possible to carry out the experimental part of this thesis.

The treatment experiment of this thesis was conducted with much appreciated help from Turku Center for Disease Modeling. I want to thank Jonna Palmu, Mona Niiranen, and Jenni Airaksinen for all the effort they put in this work.

Thank you, Markku Koulu, Ullamari Pesonen, and Sanna Soini, for all the guidance and knowledge you have given me during the master's degree programme.

Next, I would like to thank my friends Arttu Junnila, Sakari Pöysti, William Eccleshall, Riku Kuisma, and Ilari Suomalainen. Thank you, Arttu, for all the moments of laughter that made this journey lighter. It always made my days brighter knowing that you would be there working on the same floor. I am forever grateful for your tips and support through all the egg-related moments that challenged my sanity. I would also like to remind you, Arttu, that after hundreds of histology sections for this thesis, I have mastered the use of microtome, but your first section is still waiting to be cut. I would like to thank Sakari Pöysti for all the memories from student life and for the many lunch breaks we shared. I admire you, Sakke, in more ways than I can put into words and I am grateful to have you as a friend. Thank you, William, for all the support during this writing process. The coffee breaks were very much needed and your heartwarming presence never failed to ease my stress. Watching how effortlessly you manage so much work is truly inspiring. A special thanks goes to Riku Kuisma and Ilari Suomalainen. We might not

have been the strongest trio as students, but we have more than made up for it outside the university walls.

Lastly, I would like to express my greatest gratitude to my family. Mom and Dad, there are no words in the world to thank you enough for your love and support during the darkest moments of my life. You have been and always will be the foundation for all the success I have in life. I also want to thank my sister, Heidi. Your support, kindness, and understanding have meant more to me than you know. It is hard to find the words to thank the last person, who has had the biggest impact on my journey. Janne, you are an amazing brother and my idol. I have lost count on how many times I wanted to give up with my studies, but you have always given me hope and lifted me back up. I can never pay you back for everything you have done, but I hope you know how deeply grateful I am. You have always been there for me, and I hope you know that I will always be here for you.

6 ABBREVIATIONS LIST

APC Actrocyte Precursor Cell

BLI Bioluminescence imaging

CAM Chorioallantoic membrane

EDD Embryonic Development Day

EOR Extent of Resection

HGCC Human Glioblastoma Cell Culture

IR Incidence Rate

NSC Neural Stem Cell

OPC Oligendrocyte Precursor Cell

TMZ Temozolimide

UPS Ubiquitin Proteasome System

UPR Unfolded Protein Response

vWF von Willebrand Factor

REFERENCES

Abbas, T., & Dutta, A. (2009). p21 in cancer: intricate networks and multiple activities. *Nature Reviews Cancer*, *9*(6), 400–414. https://doi.org/10.1038/nrc2657

Adams, H., Chaichana, K. L., Avendaño, J., Liu, B., Raza, S. M., & Quiñones-Hinojosa, A. (2013). Adult cerebellar glioblastoma: understanding survival and prognostic factors using a population-based database from 1973 to 2009. *World Neurosurgery*, *80*(6), 237–243. https://doi.org/10.1016/J.WNEU.2013.02.010

Adams, J. (2004). The proteasome: a suitable antineoplastic target. *Nature Reviews Cancer*, *4*(5), 349–360. https://doi.org/10.1038/nrc1361

Arlt, A., Bauer, I., Schafmayer, C., Tepel, J., Müerköster, S. S., Brosch, M., Röder, C., Kalthoff, H., Hampe, J., Moyer, M. P., Fölsch, U. R., & Schäfer, H. (2009). Increased proteasome subunit protein expression and proteasome activity in colon cancer relate to an enhanced activation of nuclear factor E2-related factor 2 (Nrf2). *Oncogene*, *28*(45), 3983–3996. https://doi.org/10.1038/onc.2009.264

Ballard, C., Giang, M. H., Ostrom, Q., & Walsh, K. (2024). EPID-16. GENOMIC ANCESTRY-RELATED RISK RATIOS FOR GLIOBLASTOMA INCIDENCE AMONG GLOBAL POPULATIONS AND RACIAL/ETHNIC GROUPS WITHIN THE UNITED STATES. *Neuro-Oncology*, *26*(8). https://doi.org/10.1093/NEUONC/NOAE165.0552

Bond, A. M., Ming, G. L., & Song, H. (2015). Adult Mammalian Neural Stem Cells and Neurogenesis: Five Decades Later. *Cell Stem Cell*, *17*(4), 385–395. https://doi.org/10.1016/j.stem.2015.09.003

Brodbelt, A., Greenberg, D., Winters, T., Williams, M., Vernon, S., & Collins, V. P. (2015). Glioblastoma in England: 2007-2011. *European Journal of Cancer*, *51*(4), 533–542. https://doi.org/10.1016/J.EJCA.2014.12.014

Brown, N. F., Ottaviani, D., Tazare, J., Gregson, J., Kitchen, N., Brandner, S., Fersht, N., & Mulholland, P. (2022). Survival Outcomes and Prognostic Factors in Glioblastoma. *Cancers*, *14*(13), 3161. https://doi.org/10.3390/cancers14133161

Carrano, A., Juarez, J. J., Incontri, D., Ibarra, A., & Cazares, H. G. (2021). Sex-Specific Differences in Glioblastoma. *Cells*, *10*(7), 1783. https://doi.org/10.3390/CELLS10071783

Chakrabarti, I., Cockburn, M., Cozen, W., Wang, Y. P., & Preston-Martin, S. (2005). A population-based description of glioblastoma multiforme in Los Angeles County, 1974-1999. *Cancer*, *104*(12), 2798–2806. https://doi.org/10.1002/CNCR.21539

Chauhan, D., Catley, L., Li, G., Podar, K., Hideshima, T., Velankar, M., Mitsiades, C., Mitsiades, N., Yasui, H., Letai, A., Ovaa, H., Berkers, C., Nicholson, B., Chao, T. H., Neuteboom, S. T. C., Richardson, P., Palladino, M. A., & Anderson, K. C. (2005). A novel orally active proteasome inhibitor induces apoptosis in multiple myeloma cells with mechanisms distinct from Bortezomib. *Cancer Cell*, *8*(5), 407–419. https://doi.org/10.1016/j.ccr.2005.10.013

Chen, L., & Madura, K. (2005). Increased Proteasome Activity, Ubiquitin-Conjugating Enzymes, and eEF1A Translation Factor Detected in Breast Cancer Tissue. *Cancer Research*, *65*(13), 5599–5606. https://doi.org/10.1158/0008-5472.CAN-05-0201

Colonna, M., & Butovsky, O. (2017). Microglia Function in the Central Nervous System During Health and Neurodegeneration. *Annual Review of Immunology*, *35*, 441–468. https://doi.org/10.1146/ANNUREV-IMMUNOL-051116-052358

Cornell, J., Salinas, S., Huang, H. Y., & Zhou, M. (2021). Microglia regulation of synaptic plasticity and learning and memory. *Neural Regeneration Research*, *17*(4), 705–716. https://doi.org/10.4103/1673-5374.322423

Dahlrot, R. H., Bangsø, J. A., Petersen, J. K., Rosager, A. M., Sørensen, M. D., Reifenberger, G., Hansen, S., & Kristensen, B. W. (2021). Prognostic role of Ki-67 in glioblastomas excluding contribution from non-neoplastic cells. *Scientific Reports, 11*, 17918. https://doi.org/10.1038/s41598-021-95958-9

Damgaard, R. B. (2021). The ubiquitin system: from cell signalling to disease biology and new therapeutic opportunities. *Cell Death & Differentiation*, *28*(2), 423–426. https://doi.org/10.1038/s41418-020-00703-w

DeBord, L. C., Pathak, R. R., Villaneuva, M., Liu, H.-C., Harrington, D. A., Yu, W., Lewis, M. T., & Sikora, A. G. (2018). The chick chorioallantoic membrane (CAM) as a versatile patient-derived xenograft (PDX) platform for precision medicine and preclinical research. *American Journal of Cancer Research*, *8*(8), 1642–1660. https://pmc.ncbi.nlm.nih.gov/articles/PMC6129484/

Dhayer, M., Jordao, A., Dekiouk, S., Cleret, D., Germain, N., & Marchetti, P. (2024). Implementing Chicken Chorioallantoic Membrane (CAM) Assays for Validating Biomaterials in Tissue Engineering: Rationale and Methods. *Journal of*

Biomedical Materials Research. Part B, Applied Biomaterials, *112*(11), e35496. https://doi.org/10.1002/jbm.b.35496

Dho, Y.-S., Jung, K.-W., Ha, J., Seo, Y., Park, C.-K., Won, Y.-J., & Yoo, H. (2017). An Updated Nationwide Epidemiology of Primary Brain Tumors in Republic of Korea, 2013. *Brain Tumor Research and Treatment*, *5*(1), 16–23. https://doi.org/10.14791/BTRT.2017.5.1.16

Dobec-Meić, B., Pikija, S., Cvetko, D., Trkulja, V., Pažanin, L., Kudelić, N., Rotim, K., Pavliček, I., & Kostanjevec, R. (2006). Intracranial tumors in adult population of the Varazdin County (Croatia) 1996-2004: a population-based retrospective incidence study. *Journal of Neuro-Oncology*, *78*(3), 303–310. https://doi.org/10.1007/S11060-005-9100-2

Dobes, M., Khurana, V. G., Shadbolt, B., Jain, S., Smith, S. F., Smee, R., Dexter, M., & Cook, R. (2011). Increasing incidence of glioblastoma multiforme and meningioma, and decreasing incidence of Schwannoma (2000-2008): Findings of a multicenter Australian study. *Surgical Neurology International*, *2*, 176. https://doi.org/10.4103/2152-7806.90696

Doroszko, M., Stockgard, R., Uppman, I., Heinold, J., Voukelatou, F., Mangukiya, H. B., Millner, T. O., Skeppås, M., Ballester Bravo, M., Elgendy, R., Berglund, M., Elfineh, L., Krona, C., Kundu, S., Koltowska, K., Marino, S., Larsson, I., & Nelander, S. (2025). The invasion phenotypes of glioblastoma depend on plastic and reprogrammable cell states. *Nature Communications*, *16*, 6662. https://doi.org/10.1038/s41467-025-61999-1

Eisenbarth, D., & Wang, Y. A. (2023). Glioblastoma heterogeneity at single cell resolution. *Oncogene*, *42*(27), 2155–2165. https://doi.org/10.1038/s41388-023-02738-y

Engelhard, H. H., Villano, J. L., Porter, K. R., Stewart, A. K., Barua, M., Barker, F. G., & Newton, H. B. (2010). Clinical presentation, histology, and treatment in 430 patients with primary tumors of the spinal cord, spinal meninges, or cauda equina. *Journal of Neurosurgery: Spine*, *13*(1), 67–77. https://doi.org/10.3171/2010.3.SPINE09430

Fischer, D., Fluegen, G., Garcia, P., Ghaffari-Tabrizi-Wizsy, N., Gribaldo, L., Huang, R. Y. J., Rasche, V., Ribatti, D., Rousset, X., Pinto, M. T., Viallet, J., Wang, Y., & Schneider-Stock, R. (2022). The CAM Model—Q&A with Experts. *Cancers*, *15*(1), 191. https://doi.org/10.3390/CANCERS15010191

Friedmann-Morvinski, D., Bushong, E. A., Ke, E., Soda, Y., Marumoto, T., Singer, O., Ellisman, M. H., & Verma, I. M. (2012). Dedifferentiation of Neurons and Astrocytes by Oncogenes Can Induce Gliomas in Mice. *Science*, *338*(6110), 1080–1084. https://doi.org/10.1126/SCIENCE.1226929

Fyllingen, E. H., Bø, L. E., Reinertsen, I., Jakola, A. S., Sagberg, L. M., Berntsen, E. M., Salvesen, Ø., & Solheim, O. (2021). Survival of glioblastoma in relation to tumor location: a statistical tumor atlas of a population-based cohort. *Acta Neurochirurgica*, *163*(7), 1895–1905. https://doi.org/10.1007/S00701-021-04802-6

Grochans, S., Cybulska, A. M., Simińska, D., Korbecki, J., Kojder, K., Chlubek, D., & Baranowska-Bosiacka, I. (2022). Epidemiology of Glioblastoma Multiforme–Literature Review. *Cancers*, *14*(10), 2412. https://doi.org/10.3390/CANCERS14102412

Haupt, Y., Maya, R., Kazaz, A., & Oren, M. (1997). Mdm2 promotes the rapid degradation of p53. *Nature*, *387*(6630), 296–299. https://doi.org/10.1038/387296a0

He, W., Zhang, Z., Tan, Z. L., Liu, X. X., Wang, Z. K., Xiong, B., Shen, X. L., & Zhu, X. G. (2024). PSMB2 plays an oncogenic role in glioma and correlates to the immune microenvironment. *Scientific Reports*, *14*, 5861. https://doi.org/10.1038/s41598-024-56493-5

Janse, M. E., & Jeurissen, S. H. M. (1991). Ontogeny and Function of Two Non-Lymphoid Cell Populations in the Chicken Embryo. *Immunobiology*, *182*(5), 472–481. https://doi.org/10.1016/S0171-2985(11)80211-1

Johansson, P., Krona, C., Kundu, S., Doroszko, M., Baskaran, S., Schmidt, L., Vinel, C., Almstedt, E., Elgendy, R., Elfineh, L., Gallant, C., Lundsten, S., Ferrer Gago, F. J., Hakkarainen, A., Sipilä, P., Häggblad, M., Martens, U., Lundgren, B., Frigault, M. M., … Nelander, S. (2020). A Patient-Derived Cell Atlas Informs Precision Targeting of Glioblastoma. *Cell Reports*, *32*(2), 107897. https://doi.org/10.1016/j.celrep.2020.107897

Jung, K., Kempter, J., Prokop, G., Herrmann, T., Griessmair, M., Kim, S. H., Delbridge, C., Meyer, B., Bernhardt, D., Combs, S. E., Zimmer, C., Wiestler, B., Schmidt-Graf, F., & Metz, M. C. (2024). Quantitative Assessment of Tumor Contact with Neurogenic Zones and Its Effects on Survival: Insights beyond Traditional Predictors. *Cancers*, *16*(9), 1743. https://doi.org/10.3390/cancers16091743

Jung, K.-W., Ha, J., Lee, S. H., Won, Y.-J., & Yoo, H. (2013). An updated nationwide epidemiology of primary brain tumors in republic of Korea. *Brain Tumor Research and Treatment*, *1*(1), 16–23. https://doi.org/10.14791/BTRT.2013.1.1.16

Korja, M., Raj, R., Seppä, K., Luostarinen, T., Malila, N., Seppälä, M., Mäenpää, H., & Pitkäniemi, J. (2018). Glioblastoma survival is improving despite increasing incidence rates: a nationwide study between 2000 and 2013 in Finland. *Neuro-Oncology*, *21*(3), 370–379. https://doi.org/10.1093/NEUONC/NOY164

Krona, C., Sundström, A., Rosen, E., Kundu, S., Mangukiya, H. B., Babacic, H., Uppman, I., Skeppås, M., Larsson, I., Elfineh, L., Cao, X., Ramachandra, R., Elgendy, R., Halldorsdottir, K. R., Dave, Z., Doroszko, M., Olausson, K. H., Wikström, J., Pernemalm, M., & Nelander, S. (2025). A Phenotype-Driven Multi-Omic Atlas of Glioblastoma Invasion. *BioRxiv*, 2025.03.25.645260. https://doi.org/10.1101/2025.03.25.645260

Kruiswijk, F., Labuschagne, C. F., & Vousden, K. H. (2015). p53 in survival, death and metabolic health: a lifeguard with a licence to kill. *Nature Reviews Molecular Cell Biology*, *16*(7), 393–405. https://doi.org/10.1038/nrm4007

Lee, J., Kotliarova, S., Kotliarov, Y., Li, A., Su, Q., Donin, N. M., Pastorino, S., Purow, B. W., Christopher, N., Zhang, W., Park, J. K., & Fine, H. A. (2006). Tumor stem cells derived from glioblastomas cultured in bFGF and EGF more closely mirror the phenotype and genotype of primary tumors than do serum-cultured cell lines. *Cancer Cell*, *9*(5), 391–403. https://doi.org/10.1016/J.CCR.2006.03.030

Liu, C., Sage, J. C., Miller, M. R., Verhaak, R. G. W., Hippenmeyer, S., Vogel, H., Foreman, O., Bronson, R. T., Nishiyama, A., Luo, L., & Zong, H. (2011). Mosaic analysis with double markers reveals tumor cell of origin in glioma. *Cell*, *146*(2), 209–221. https://doi.org/10.1016/j.cell.2011.06.014

Liu, T. T., Achrol, A. S., Mitchell, L. A., Du, W. A., Loya, J. J., Rodriguez, S. A., Feroze, A., Westbroek, E. M., Yeom, K. W., Stuart, J. M., Chang, S. D., Harsh, G. R., & Rubin, D. L. (2016). Computational Identification of Tumor Anatomic Location Associated with Survival in 2 Large Cohorts of Human Primary Glioblastomas. *AJNR: American Journal of Neuroradiology*, *37*(4), 621–628. https://doi.org/10.3174/AJNR.A4631

Liu, X., Ying, J., Wang, X., Zheng, Q., Zhao, T., Yoon, S., Yu, W., Yang, D., Fang, Y., & Hua, F. (2021). Astrocytes in Neural Circuits: Key Factors in Synaptic

Regulation and Potential Targets for Neurodevelopmental Disorders. *Frontiers in Molecular Neuroscience*, *14*. https://doi.org/10.3389/fnmol.2021.729273

Lottaz, C., Beier, D., Meyer, K., Kumar, P., Hermann, A., Schwarz, J., Junker, M., Oefner, P. J., Bogdahn, U., Wischhusen, J., Spang, R., Storch, A., & Beier, C. P. (2010). Transcriptional profiles of CD133+ and CD133- glioblastoma-derived cancer stem cell lines suggest different cells of origin. *Cancer Research*, *70*(5), 2030–2040. https://doi.org/10.1158/0008-5472.CAN-09-1707

Meneceur, S., Linge, A., Meinhardt, M., Hering, S., Löck, S., Bütof, R., Krex, D., Schackert, G., Temme, A., Baumann, M., Krause, M., & von Neubeck, C. (2020). Establishment and Characterisation of Heterotopic Patient-Derived Xenografts for Glioblastoma. *Cancers*, *12*(4), 871. https://doi.org/10.3390/CANCERS12040871

Miranda-Filho, A., Piñeros, M., Soerjomataram, I., Deltour, I., & Bray, F. (2016). Cancers of the brain and CNS: global patterns and trends in incidence. *Neuro-Oncology*, *19*(2), 270–280. https://doi.org/10.1093/NEUONC/NOW166

Miyakoshi, A., Ubukata, N., Miyake, H., Shoji-Asahina, A., Dote, H., Ohata, E., Funaki, D., Ichikawa, Y., Imaichi, Y., Oshima, M., Hawke, P., & Nakatani, E. (2024). Risk factors for glioblastoma in adults in Japan: an exploratory cohort study based on the Shizuoka Kokuho Database, the Shizuoka study. *Journal of Neuro-Oncology*, *166*(2), 341–349. https://doi.org/10.1007/S11060-024-04566-W

Nagai, H., Tanoue, Y., Nakamura, T., Chan, C. J. J., Yamada, S., Saitou, M., Fukuda, T., & Sheng, G. (2022). Mesothelial fusion mediates chorioallantoic membrane formation. *Philosophical Transactions of the Royal Society B, Biological Sciences*, *377*(1865). https://doi.org/10.1098/RSTB.2021.0263

Natukka, T., Raitanen, J., Haapasalo, H., & Auvinen, A. (2019). Incidence trends of adult malignant brain tumors in Finland, 1990-2016. *Acta Oncologica*, *58*(7), 990–996. https://doi.org/10.1080/0284186X.2019.1603396

Neftel, C., Laffy, J., Filbin, M. G., Hara, T., Shore, M. E., Rahme, G. J., Richman, A. R., Silverbush, D., Shaw, M. L., Hebert, C. M., Dewitt, J., Gritsch, S., Perez, E. M., Gonzalez Castro, L. N., Lan, X., Druck, N., Rodman, C., Dionne, D., Kaplan, A., … Suvà, M. L. (2019). An Integrative Model of Cellular States, Plasticity, and Genetics for Glioblastoma. *Cell*, *178*(4), 835-849. https://doi.org/10.1016/j.cell.2019.06.024

Nowak-Sliwinska, P., Segura, T., & Iruela-Arispe, M. L. (2014). The chicken chorioallantoic membrane model in biology, medicine and bioengineering. *Angiogenesis*, *17*(4), 779–804. https://doi.org/10.1007/S10456-014-9440-7

Obeng, E. A., Carlson, L. M., Gutman, D. M., Harrington, W. J., Lee, K. P., & Boise, L. H. (2006). Proteasome inhibitors induce a terminal unfolded protein response in multiple myeloma cells. *Blood*, *107*(12), 4907–4916. https://doi.org/10.1182/BLOOD-2005-08-3531

Obernier, K., & Alvarez-Buylla, A. (2019). Neural stem cells: origin, heterogeneity and regulation in the adult mammalian brain. *Development (Cambridge, England)*, *146*(4), dev156059. https://doi.org/10.1242/DEV.156059

Ostrom, Q. T., Gittleman, H., Farah, P., Ondracek, A., Chen, Y., Wolinsky, Y., Stroup, N. E., Kruchko, C., & Barnholtz-Sloan, J. S. (2013). CBTRUS Statistical Report: Primary Brain and Central Nervous System Tumors Diagnosed in the United States in 2006-2010. *Neuro-Oncology*, *15*(Suppl 2), ii1–ii56. https://doi.org/10.1093/NEUONC/NOT151

Ostrom, Q. T., Price, M., Neff, C., Cioffi, G., Waite, K. A., Kruchko, C., & Barnholtz-Sloan, J. S. (2023). CBTRUS Statistical Report: Primary Brain and Other Central Nervous System Tumors Diagnosed in the United States in 2016—2020. *Neuro-Oncology*, *25*(Suppl 4), iv1–iv99. https://doi.org/10.1093/NEUONC/NOAD149

Park, J., Cho, J., & Song, E. J. (2020). Ubiquitin–proteasome system (UPS) as a target for anticancer treatment. *Archives of Pharmacal Research*, *43*(11), 1144–1161. https://doi.org/10.1007/S12272-020-01281-8

Piva, R., Cancelli, I., Cavalla, P., Bortolotto, S., Dominguez, J., Draetta, G. F., & Schiffer, D. (1999). Proteasome-dependent degradation of p27/kip1 in gliomas. *Journal of Neuropathology and Experimental Neurology*, *58*(7), 691–696. https://doi.org/10.1097/00005072-199907000-00002

Ribatti, D. (2014). The chick embryo chorioallantoic membrane as a model for tumor biology. *Experimental Cell Research*, *328*(2), 314–324. https://doi.org/10.1016/j.yexcr.2014.06.010

Ribatti, D. (2022). The chick embryo chorioallantoic membrane as an experimental model to study in vivo angiogenesis in glioblastoma multiforme. *Brain Research Bulletin*, *182*, 26–29. https://doi.org/10.1016/J.BRAINRESBULL.2022.02.005

Roos-Mattjus, P., & Sistonen, L. (2004). The ubiquitin-proteasome pathway. *Annals of Medicine*, *36*(4), 285–295. https://doi.org/10.1080/07853890310016324

Saric, T., Graef, C. I., & Goldberg, A. L. (2004). Pathway for Degradation of Peptides Generated by Proteasomes. *Journal of Biological Chemistry*, *279*(45), 46723–46732. https://doi.org/10.1074/JBC.M406537200

Singh, S., Dey, D., Barik, D., Mohapatra, I., Kim, S., Sharma, M., Prasad, S., Wang, P., Singh, A., & Singh, G. (2025). Glioblastoma at the crossroads: current understanding and future therapeutic horizons. *Signal Transduction and Targeted Therapy*, *10*, 213. https://doi.org/10.1038/s41392-025-02299-4

Sloan, A. R., Silver, D. J., Kint, S., Gallo, M., & Lathia, J. D. (2024). Cancer stem cell hypothesis 2.0 in glioblastoma: Where are we now and where are we going? *Neuro-Oncology*, *26*(5), 785–795. https://doi.org/10.1093/NEUONC/NOAE011

Soave, C. L., Guerin, T., Liu, J., & Dou, Q. P. (2017). Targeting the ubiquitin-proteasome system for cancer treatment: discovering novel inhibitors from nature and drug repurposing. *Cancer and Metastasis Reviews*, *36*(4), 717–736. https://doi.org/10.1007/S10555-017-9705-X

Sottoriva, A., Spiteri, I., Piccirillo, S. G. M., Touloumis, A., Collins, V. P., Marioni, J. C., Curtis, C., Watts, C., & Tavaré, S. (2013). Intratumor heterogeneity in human glioblastoma reflects cancer evolutionary dynamics. *Proceedings of the National Academy of Sciences of the United States of America*, *110*(10), 4009–4014. https://doi.org/10.1073/pnas.1219747110

Stupp, R., Mason, W. P., van den Bent, M. J., Weller, M., Fisher, B., Taphoorn, M. J. B., Belanger, K., Brandes, A. A., Marosi, C., Bogdahn, U., Curschmann, J., Janzer, R. C., Ludwin, S. K., Gorlia, T., Allgeier, A., Lacombe, D., Cairncross, J. G., Eisenhauer, E., & Mirimanoff, R. O. (2005). Radiotherapy plus concomitant and adjuvant temozolomide for glioblastoma. *The New England Journal of Medicine*, *352*(10), 987–996. https://doi.org/10.1056/NEJMOA043330

Suvà, M. L., Rheinbay, E., Gillespie, S. M., Patel, A. P., Wakimoto, H., Rabkin, S. D., Riggi, N., Chi, A. S., Cahill, D. P., Nahed, B. V., Curry, W. T., Martuza, R. L., Rivera, M. N., Rossetti, N., Kasif, S., Beik, S., Kadri, S., Tirosh, I., Wortman, I., … Bernstein, B. E. (2014). Reconstructing and reprogramming the tumor-propagating potential of glioblastoma stem-like cells. *Cell*, *157*(3), 580–594. https://doi.org/10.1016/j.cell.2014.02.030

Thrower, J. S., Hoffman, L., Rechsteiner, M., & Pickart, C. M. (2000). Recognition of the polyubiquitin proteolytic signal. *The EMBO Journal*, *19*(1), 94–102. https://doi.org/10.1093/EMBOJ/19.1.94

Tolcher, A. W., Gerson, S. L., Denis, L., Geyer, C., Hammond, L. A., Patnaik, A., Goetz, A. D., Schwartz, G., Edwards, T., Reyderman, L., Statkevich, P., Cutler, D. L., & Rowinsky, E. K. (2003). Marked inactivation of O6-alkylguanine-DNA alkyltransferase activity with protracted temozolomide schedules. *British Journal of Cancer*, *88*(7), 1004–1011. https://doi.org/10.1038/SJ.BJC.6600827

Verhaak, R. G. W., Hoadley, K. A., Purdom, E., Wang, V., Qi, Y., Wilkerson, M. D., Miller, C. R., Ding, L., Golub, T., Mesirov, J. P., Alexe, G., Lawrence, M., O'Kelly, M., Tamayo, P., Weir, B. A., Gabriel, S., Winckler, W., Gupta, S., Jakkula, L., … Hayes, D. N. (2010). An integrated genomic analysis identifies clinically relevant subtypes of glioblastoma characterized by abnormalities in PDGFRA, IDH1, EGFR and NF1. *Cancer Cell*, *17*(1), 98–110. https://doi.org/10.1016/J.CCR.2009.12.020

Vlachostergios, P. J., Voutsadakis, I. A., & Papandreou, C. N. (2012). The ubiquitin-proteasome system in glioma cell cycle control. *Cell Division*, *7*, 18. https://doi.org/10.1186/1747-1028-7-18

Walker, E. V., Davis, F. G., Shaw, A., Louchini, R., Shack, L., Woods, R., Kruchko, C., Spinelli, J., Guiot, M. C., Perry, J., Melin, B., Barnholtz-Sloan, J., Turner, D., King, M. J., Hannah, H., & Bryant, H. (2019). Malignant primary brain and other central nervous system tumors diagnosed in Canada from 2009 to 2013. *Neuro-Oncology*, *21*(3), 360–369. https://doi.org/10.1093/NEUONC/NOY195

Wang, Q., Hu, B., Hu, X., Kim, H., Squatrito, M., Scarpace, L., deCarvalho, A. C., Lyu, S., Li, P., Li, Y., Barthel, F., Cho, H. J., Lin, Y. H., Satani, N., Martinez-Ledesma, E., Zheng, S., Chang, E., Sauvé, C. E. G., Olar, A., … Verhaak, R. G. W. (2017). Tumor evolution of glioma intrinsic gene expression subtype associates with immunological changes in the microenvironment. *Cancer Cell*, *32*(1), 42–56. https://doi.org/10.1016/J.CCELL.2017.06.003

Wang, Q., Wu, H., Hu, J., Fu, H., Qu, Y., Yang, Y., Cai, Q., Efimov, A., Wu, M., Yen, T., Wang, Y., & Yang, Z. J. (2021). Nestin is required for spindle assembly and cell cycle progression in glioblastoma cells. *Molecular Cancer Research*, *19*(10), 1651–1665. https://doi.org/10.1158/1541-7786.MCR-20-0994

Wang, Y., Xue, W., Pustovalova, M., Kuzmin, D. V., & Leonov, S. (2025). Chick Embryo Chorioallantoic Membrane (CAM) Model for Cancer Studies and Drug Evaluation. *Frontiers in Bioscience (Landmark Edition)*, *30*(5), 37456. https://doi.org/10.31083/FBL37456

Wick, W., Platten, M., Meisner, C., Felsberg, J., Tabatabai, G., Simon, M., Nikkhah, G., Papsdorf, K., Steinbach, J. P., Sabel, M., Combs, S. E., Vesper, J., Braun, C., Meixensberger, J., Ketter, R., Mayer-Steinacker, R., Reifenberger, G., & Weller, M. (2012). Temozolomide chemotherapy alone versus radiotherapy alone for malignant astrocytoma in the elderly: The NOA-08 randomised, phase 3 trial. *The Lancet Oncology*, *13*(7), 707–715. https://doi.org/10.1016/S1470-2045(12)70164-X

Wilson, T. A., Karajannis, M. A., & Harter, D. H. (2014). Glioblastoma multiforme: State of the art and future therapeutics. *Surgical Neurology International*, *5*, 64. https://doi.org/10.4103/2152-7806.132138

Wolbers, J. G. (2014). Novel strategies in glioblastoma surgery aim at safe, supra-maximum resection in conjunction with local therapies. *Chinese Journal of Cancer*, *33*(1), 8–15. https://doi.org/10.5732/CJC.013.10219

Xie, Y., Bergström, T., Jiang, Y., Johansson, P., Marinescu, V. D., Lindberg, N., Segerman, A., Wicher, G., Niklasson, M., Baskaran, S., Sreedharan, S., Everlien, I., Kastemar, M., Hermansson, A., Elfineh, L., Libard, S., Holland, E. C., Hesselager, G., Alafuzoff, I., … Uhrbom, L. (2015). The Human Glioblastoma Cell Culture Resource: Validated Cell Models Representing All Molecular Subtypes. *EBioMedicine*, *2*(10), 1351–1363. https://doi.org/10.1016/j.ebiom.2015.08.026

Zhang, N., Yi, R., Zhong, F., Lu, Y., Chen, W., Ke, Z., Zhang, Y., Zhou, L., Wang, P., & Li, W. (2025). Oligodendrocytes and myelination: pioneering new frontiers in cognitive neuroscience. *Frontiers in Neuroscience*, *19*, 1618468. https://doi.org/10.3389/FNINS.2025.1618468

USE OF ARTIFICIAL INTELLIGENCE

AI-based tools, such as Keenious and Scopus AI, were used to find relevant publications for this thesis. OpenAI was used to summarise these articles and process the information within them. All publications and their information were critically evaluated by the author. The text, ideas, and conclusions in this thesis are author's own.

APPENDICES

Appendix 1

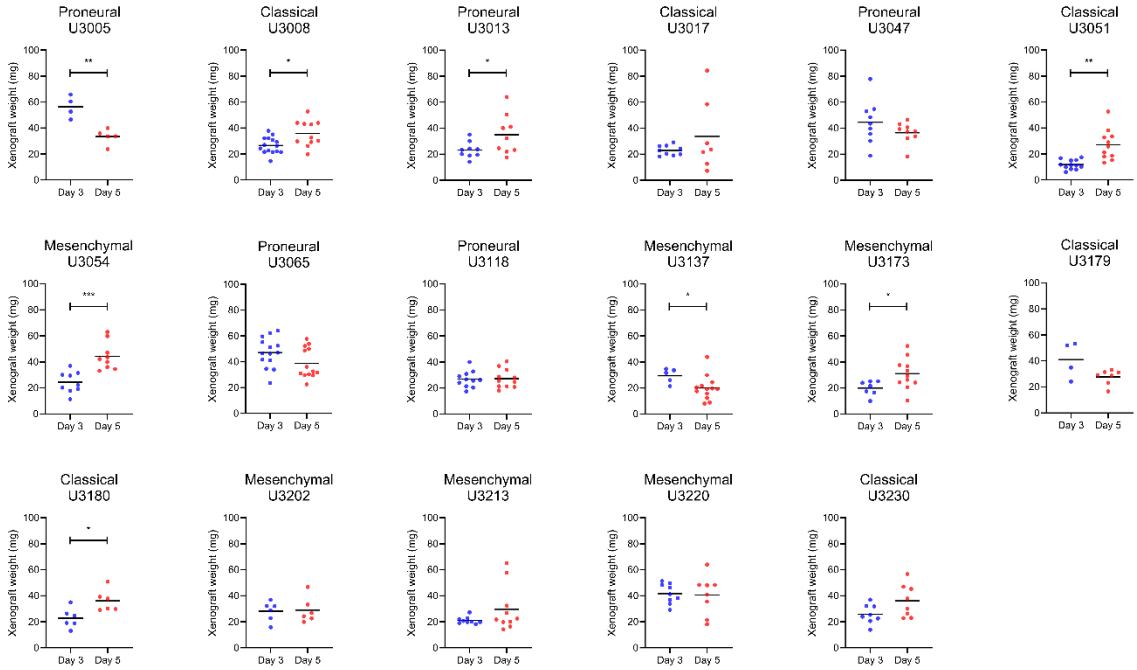

Tumour weight progression of xenografts from all glioblastoma cell lines.

Appendix 2

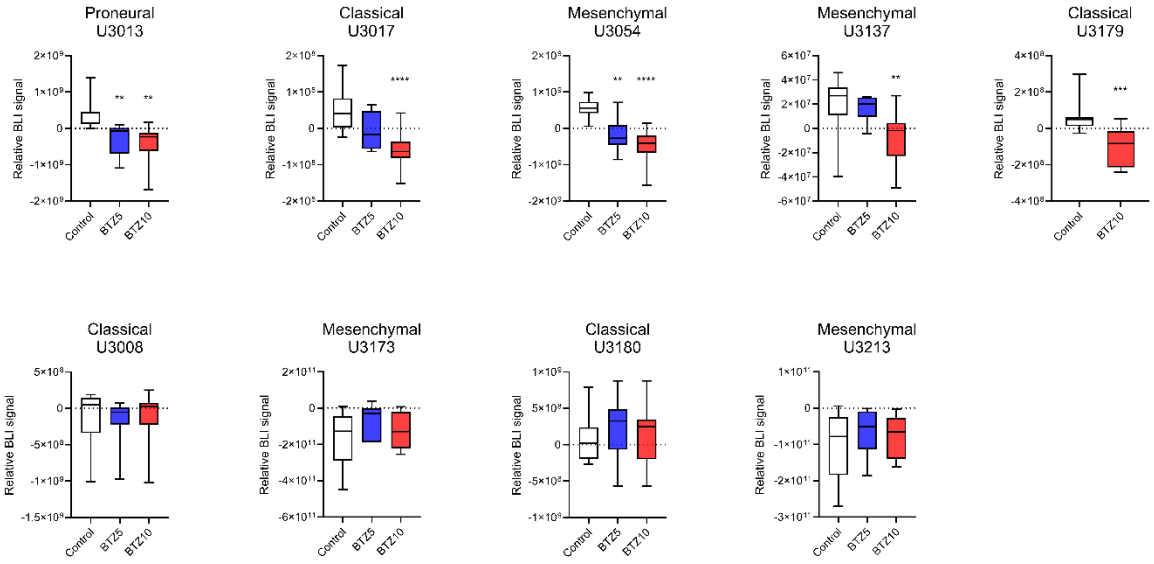

Relative BLI data of xenografts from all glioblastoma cell lines.

Appendix 3

IVIS imaging sequence and parameters.

Fluorescence	**Emission/Excitation**	**F stop**	**Exposure (s)**	
1.	500/465	2	2	
2.	620/500	2	Auto	
Bioluminescence	**Delay (min)**	**F stop**	**Exposure (s)**	**Binning**
1.	3.5	1	1	8
2.		1	2	8
3.		1	Auto	8
4.	1	1	1	8
5.		1	2	8
6.		1	Auto	8
7.	1	1	1	8
8.		1	2	8
9.		1	Auto	8
10.	1	1	1	8
11.		1	2	8
12.		1	Auto	8
13.	1	1	1	8
14.		1	2	8
15.		1	Auto	8
16.		1	1	16
17.		1	2	16
18.		1	Auto	16
19.		1	1	4
20.		1	2	4
21.		1	Auto	4